



HAL
open science

Experimental simulation of magma mixing at high pressure

Mickaël Laumonier, Bruno Scaillet, Laurent Arbaret, Rémi Champallier

► **To cite this version:**

Mickaël Laumonier, Bruno Scaillet, Laurent Arbaret, Rémi Champallier. Experimental simulation of magma mixing at high pressure. *Lithos*, 2014, 196-197, pp.281-300. 10.1016/j.lithos.2014.02.016 . insu-00955227

HAL Id: insu-00955227

<https://insu.hal.science/insu-00955227>

Submitted on 4 Mar 2014

HAL is a multi-disciplinary open access archive for the deposit and dissemination of scientific research documents, whether they are published or not. The documents may come from teaching and research institutions in France or abroad, or from public or private research centers.

L'archive ouverte pluridisciplinaire **HAL**, est destinée au dépôt et à la diffusion de documents scientifiques de niveau recherche, publiés ou non, émanant des établissements d'enseignement et de recherche français ou étrangers, des laboratoires publics ou privés.

EXPERIMENTAL SIMULATION OF MAGMA MIXING AT HIGH PRESSURE

Mickael Laumonier^{1*}, Bruno Scaillet¹, Laurent Arbaret¹, Rémi Champallier¹

¹CNRS-Université d'Orléans-BRGM, ISTO, UMR 7327, 45071, Orléans, France

Corresponding author: M LAUMONIER: mickael.laumonier@univ-orleans.fr

*present address : mickael.laumonier@uni-bayreuth.de

ABSTRACT

Magma mixing features are observed in many plutonic and volcanic environments. They result from the juxtaposition of two chemically contrasted magmas, usually during the replenishment of a magmatic reservoir, but also syn-eruptively within the conduit. Despite its ubiquity, only a few experimental studies have explored mixing between magmas. Existing data have been mostly acquired at atmospheric pressure and high shear rates ($>10^{-1} \text{ s}^{-1}$), which differ from those accompanying magma mixing in reservoirs. To fill this gap, we performed high pressure mixing experiments at strain rates ranging from $4 \cdot 10^{-4}$ to $1 \cdot 10^{-3} \text{ s}^{-1}$. Layers of a synthetic crystal-free hapltonalite and a natural partially-molten basalt were juxtaposed in a Paterson apparatus at 300 MPa, and deformed between 900 and 1200°C. The experiments shed light on the first stages of magma mixing and illustrate the role and behavior of crystals, either pre-existing or newly grown. Experiments evidence a rheological threshold for mafic material disruption, which sets in abruptly as its melt fraction exceeds 50%, which in the experiments occurs in the narrow temperature interval 1160-1170°C. Below this threshold, plagioclase crystals in the mafic magma form a rigid touching network and all the deformation is accommodated by the less viscous felsic layer. Above it the crystal network collapses, allowing typical mingling/mixing features to appear altogether, such as enclaves, melt filaments or single xenocrysts isolated into the felsic end-member, coexisting with newly grown phases (plagioclase and pyroxene) whose compositions spread out over considerable ranges. The pre-existing fabric of the mafic magma is only slightly affected by deformation,

altogether providing few clues on either the regime or geometry of applied deformation during the magmatic stage.

1. INTRODUCTION

The mixing between magmas with different chemical compositions is a process commonly observed in nature (see [Perugini & Poli, 2012](#)) as illustrated by the widespread occurrence of (1) hybrid compositions (e.g., [Castro et al., 1990](#); [Eichelberger 2010](#)), (2) enclaves (e.g., [Armienti et al., 1983](#); [Civetta et al., 1997](#); [Davi et al., 2010](#)), (3) chemically banded rocks (e.g., [Druitt et al., 1999](#); [Pons et al., 2006](#)) or (4) crystals in disequilibrium in their host (e.g., [Sakuyama, 1979](#); [Pal et al., 2007](#)). Such mixing features are described in either volcanic ([Anderson, 1976](#); [Blake, 1984](#); [De Rosa et al., 1996](#); [Coombs et al., 2002](#); [De Rosa et al., 2002](#); [Perugini et al., 2004](#); [Martel et al., 2006](#); [Martin et al., 2006a,b](#); [Martel & Poussineau, 2007](#); [Appel et al., 2009](#); [Woods & Cowan, 2009](#); [Davi et al., 2010](#)) or plutonic (e.g., [Bacon, 1986](#); [Castro et al., 1990](#); [Smith, 2000](#); [Dokukina et al., 2010](#)) contexts. In most cases, mixing results from the juxtaposition of two chemically contrasted magmas during the replenishment of a reservoir through the injection of mafic dykes (e.g., [Sparks et al., 1977](#); [Sakuyama, 1979](#); [Bacon, 1986](#); [Civetta et al., 1991](#); [Nakamura, 1995](#); [Mandeville et al., 1996](#); [Pallister et al., 1996](#); [Petford, 1996](#); [Venezky & Rutherford, 1997](#); [Clynne, 1999](#); [Browne et al., 2006](#); [Pal et al., 2007](#); [Eichelberger, 2010](#); [Ruprecht & Bachmann, 2010](#)). Owing to the frequent occurrence of mixing in erupted rocks, magma mixing has been often proposed as one of the main trigger of volcanic eruptions (e.g., [Sparks et al., 1977](#); [Pallister et al., 1996](#); [Eichelberger, 2010](#); [Kent et al., 2010](#); [Ruprecht & Bachmann, 2010](#); [La Felice & Landi, 2011](#); [Druitt et al., 2012](#)). The replenishment of a cooling silicic reservoir by a hot basic magma ([Wiebe, 1996](#); [Miller et al., 1999](#)) induces changes in temperature, which affect magma crystallinity, hence its viscosity and density ([Sparks et al., 1977](#); [Eichelberger, 1980](#); [Huppert et al., 1984](#)). The viscosity is critical for magma mixing because a low viscosity contrast between end-members favors their mixing, as demonstrated by various analogical experiments (e.g., [Huppert et al., 1984](#); [Blake & Ivey, 1986](#); [Koyaguchi & Blake, 1989](#); [Jellinek et al., 1999](#); [Sato & Sato, 2009](#)).

Numerical or theoretical approaches have also emphasized the importance of physical parameters in controlling mixing efficiency (e.g., Sparks & Marshall, 1986; Bergantz; 2000; Perugini et al., 2004).

In contrast to these analogical and numerical efforts, experimental investigation of mixing phenomena at high P and T has remained limited, owing to the obvious technical difficulties in implementing deformation apparatus at elevated pressures. In fact, high pressure studies about magma mixing have been so far restricted to static conditions (e.g., Watson & Jurewicz, 1984; Carroll & Wyllie, 1989; Wyllie et al., 1989; Van der Laan & Wyllie, 1993; Erdmann et al., 2012) and have mostly addressed chemical aspects. Deformation studies are only a few and have been performed at 1 bar, thus at relatively high temperatures, generally at very high strain rates, and considering mostly melt mixtures, which limit their direct application to natural systems, though providing valuable insights on mixing mechanisms. In a pioneer study, Kouchi & Sunagawa (1982) deformed natural basalt and dacite and produced enclaves and a hybrid intermediate melt at 1200°C and atmospheric pressure. The andesite so produced was barely homogeneous while the dacite ended up being chemically zoned. The authors evidenced the enhancement of mixing by the presence of rotating crystals in melt at high strain rates. More recently, De Campos et al. (2008, 2011) produced mingling textures by deforming contrasted synthetic melts at 1,400°C and atmospheric pressure under high strain rates as well ($>10^{-1} \text{ s}^{-1}$), showing that forceful convection allows mixing between melts whose respective viscosities differ by 3 orders of magnitude, while analogue models suggest that mixing is greatly inhibited when the viscosities of both end members differs considerably (e.g., Huppert et al., 1984). It is important to note that the shear rate of 1 bar mixing experiments on silicate magmas, generally obtained in rotating apparatus, exceeds by several orders of magnitude those expected to occur at depth (ca. 10^{-7} s^{-1} , Williams and Tobisch, 1994; 10^{-12} to 10^{-2} s^{-1} , Albers et al., 2005 and references therein; Fig. 1A): Kouchi & Sunagawa (1982, 1985) experiments were performed applying 48 rotations per minute (during 2 hours), whilst De Campos et al. (2011) applied a minimum rate of about 4 tours every hour which the latter being

broadly equivalent to a strain rate of 10^{-1} s^{-1} . Thus, although clearly promoting mixing and having some relevance to volcanic contexts, the dynamic conditions of these experiments cannot be used straightforwardly to infer those prevailing in many natural systems, particularly in slowly cooling plutons where most mixing textures are documented (e.g., Barbarin, 2005; Blundy & Sparks, 1992). For instance, the fastest plutonic strain rates calculated by Albertz et al. (2005) occur near the pluton margins and close to the feeding dykes (10^{-4} to 10^{-2} s^{-1} , Fig. 1A). Recent analogical experiments have concluded that enclave breakup in convective reservoirs imply convective velocities $> 10^{-2} \text{ m/s}$ (Hodge et al., 2012) which correspond to shear rates at the high end of the range indicated above.

In this study we present mingling and mixing textures obtained during torsion experiments at high pressure and relatively slow strain rates, from 10^{-5} to 10^{-3} s^{-1} , by juxtaposition of two contrasted magmas, differing both by their chemical composition and crystal fraction. This work explores in particular mixing and mingling caused by the replenishment of a magmatic reservoir via injections, during which shearing occurs at the contact between end-members (Fig. 1A). As will be shown, our results document the incipient stages of dynamic interaction between two contrasted magmas. Particular attention is paid to the role and behavior of crystals during mixing. Although following Bacon (1986) and Sparks & Marshall (1986), it is common practice to use “mingling” for mechanical mixing and “mixing” for chemical processes, here we use the sole term of mixing. A purely physical mixing never occurs, as chemical diffusion will always proceed to some extent, depending on temperature and time lapse after the onset of contact between end-members. Magmas exposing mingling textures are those that have cooled fast enough to impede chemical homogenization, regardless of the process involved (static, ie purely diffusive, or dynamic where homogenization is physically enhanced via folding and stretching which shorten diffusion distances). We used dry magmas in an effort to limit quench crystallization (ie water decreases melt viscosity, see Laumonier et al. in preparation), which was not however fully avoided. Scanning Electronic Microscope (SEM) pictures along with chemical analyses shed light on textures

produced during the first stages of magma mixing. A separate study explores the role of water on mixing using a similar experimental procedure (Laumonier et al., submitted). The present work focuses on the documentation of textures produced during deformation experiments juxtaposing contrasted dry compositions. The rheological data pertaining to both dry and hydrous studies, together with their general implications, will be presented elsewhere (Laumonier et al. in preparation).

2. EXPERIMENTAL PROCEDURE

2.1. Starting materials and analytical techniques

Starting materials for experiments were a natural basalt from Santorini Volcano and a synthetic haplotonalitic glass. The mafic end-member is a natural holocrystalline basalt sampled in the massive part of the Cape Balos flow on Santorini volcano, Greece (Nicholls, 1971; Druitt et al., 1999; “whole rock” in Table 1). Plagioclase, olivine and clinopyroxene are the main phenocrysts while Fe-Ti oxides and orthopyroxene occur as accessory phases. Modal proportions of the main phases were determined from Scanning Electron Microscope image analyses (SEM Jeol with an acceleration voltage of 15 to 22kV and a current of 5 to 8 nA; Fig. 2). Pyroxenes, olivine and Fe-Ti oxides represent 25% of the crystal load, the remaining being made of plagioclase. Plagioclase cores (An78) are usually surrounded by a less calcic rim (An48 to An70; Table1). From the textural viewpoint, plagioclase phenocrysts define a connected crystal framework (e.g., Philpotts et al., 1998; Martin et al., 2006a), isolating patches of clinopyroxene crystals (Fig.2A; Table 1). Plagioclase cores and rims correspond to ~70% and ~30% (volume), respectively, of the plagioclase population. The length of plagioclase core ranges from a couple of μm up to 500 μm while the crystal width typically varies between 20 and 40 μm . The local plagioclase fabric was determined by digitising the edges of crystals using the Intercept methods of the software Intercept2003 (Launeau, 2004). On Figure 2A are shown the long axes of local ellipsoids. The plagioclase

microphenocrysts define altogether a weak shape preferred orientation (SPO), locally affected by isolated large olivine (Fo72 to Fo78) phenocrysts. The oriented long axes of the 124 local ellipsoids are reported on a rose diagram and define a fabric intensity of 1.94 (1 for an isotropic fabric). The angular distribution is dominated by low values ($< 20^\circ$ and $> 170^\circ$, zero being the vertical reference). The aggregates of clinopyroxene (augite) range up to 300 μm in diameter, in association with oxides (Fig.2A, Table 1). All the basalt layers cored and subsequently used as disks in deformation experiments in this study displayed this light SPO fabric, which turned out to be often perpendicular to the applied shear, though not in a systematic way (compare top and bottom Fig. 4b).

The felsic end-member is a synthetic haplotonalitic glass produced by Schott A.G. (Germany, Table 1). Its simplified chemical composition, close to some natural felsic compositions (trachyte to rhyolite), allows plagioclase crystallization until 1230°C under dry conditions. This composition has been extensively used in previous experiments and its melting behaviour is well known, in particular under hydrous conditions (Laumonier et al., 2011; Picard et al., 2011; 2013). To allow comparison between the dry (this study) and wet (Laumonier et al., submitted) results we hence kept using the same silicic end-member in both studies. Depending on crystal fraction, the anorthite content of plagioclase varies from $\sim\text{An}20$ to $\sim\text{An}34$ (Picard, 2009). However, without water, the starting felsic material has slow crystallization kinetics and remains essentially free of crystals after short time experiments, except near interfaces (see below).

2.2. Experimental strategy

We first conducted partial melting static experiments at different temperatures on basalt in order to define its melt fraction curve. This allowed us to define the temperature interval at which the viscosity contrast between basalt and haplotonalite is the lowest (Laumonier et al., in preparation), hence favoring mixing. Experiments were done in an internally heated pressure vessel at a total pressure of 300 MPa, temperatures from 1000 to 1200°C and oxygen fugacity $f\text{O}_2 \approx \text{NNO}$. For each temperature, a cylinder cored out from the basalt was introduced into an Au-Pd capsule,

which was welded shut at both ends. Then, the capsule was placed in the isothermal zone of the furnace ($\Delta T^{\circ}\text{C} < 2^{\circ}\text{C}$). The different syntheses lasted 5 hours at the target conditions and were ended by drop quench (Holloway et al., 1992; Di Carlo et al., 2006) to avoid quench crystallization. The results show that the crystal fraction decreases smoothly with temperature, reaching a fraction lower than 50 % at temperatures higher than 1170°C (Fig.2B and 3A). After 5 hours at 1200°C, the basalt has largely melted out, with only 12-13% of the solid phase (mostly plagioclase) remaining (Fig.2C), while at 1170°C, some clinopyroxene persists in addition to plagioclase and new olivine crystallizes (Fig. 2B). Near 1200°C, the experimental melt fraction is close to that predicted by the MELTS software (Ghiorso & Sack, 1995) suggesting that, at such high temperatures, the kinetics is fast enough to allow the system to reach close-to-equilibrium conditions. For the haplotonalite, no crystals were observed in the range of 1150-1200°C, except at the interface with the jacket which favored heterogeneous crystal nucleation.

On the basis of these results, we calculated the theoretical viscosity evolution of each end-member in the explored temperature range by using the model of Giordano et al. (2008; Fig. 3B). The effect of crystals was implemented by using the data sets of Champallier et al. (2008), Picard et al. (2011), Picard (2009), and the model of Roscoe (1952), based on Costa et al. (2009) (see Laumonier et al., in preparation). The viscosity curves of both end-members cross at around 1170°C (Fig. 3B). Assuming that magma mixing is enhanced when both end-members have similar viscosities (e.g., Huppert et al., 1984; Blake & Ivey, 1986; Koyaguchi & Blake, 1989; Jellinek et al., 1999; Sato & Sato, 2009), we performed most torsion experiments in the 1170-1200°C temperature range, although lower temperatures were also explored at preliminary stages. Measurements of rheological behavior (viscosity) during deformation experiments on either single or composite samples, confirmed these calculations and predictions (see Laumonier et al., in preparation). Successful and one unsuccessful mixing experiments are presented.

2.3. Experimental set up

The samples are composed of 4 stacked disks (13.5 to 15.0 mm in diameter, 5.3 to 8.6 mm in length) alternating in composition, starting with a haplotonalitic upper layer, as shown in Fig. 1B, thus allowing 3 interfaces between both end-members. The stack is sandwiched between alumina spacers, alumina and zirconia pistons, and located in the isothermal zone of the furnace ($\pm 2^\circ\text{C}$ on 35 mm length). An iron jacket (strengthened by a steel jacket) perfectly drapes the sample at high pressure. To avoid chemical reactions with the jacket, a platinum foil was inserted between the sample and the iron jacket. The column so prepared was inserted in a Paterson press (Paterson instrument, Australian Scientific Instruments) at ISTO and pressurized at room temperature up to 210 MPa, after which temperature was raised, reaching the desired temperature (900 to 1200°C) and pressure (300 MPa) in less than 1 hour. Once the target temperature was reached, a 1-hour lap-time was allowed for sample equilibration before torsion started and applied during 2-4 hours (Table 2). Torsion was stopped before jacket full failure (whose onset is revealed by a drastic decrease of the applied torque) and the sample was quenched at constant pressure at a rate of $\sim 60^\circ\text{C}/\text{min}$. Torsion deformation applied on such a cylindrical stack simulates simple shear conditions such as that occurring at the edges of mafic dyke propagating into a felsic reservoir (Fig. 1A). Six torsion experiments were conducted at different strain rates ($3 \cdot 10^{-4} < \dot{\gamma} < 1 \cdot 10^{-3} \text{ s}^{-1}$) and for various finite bulk strain ($3.1 < \gamma < 4.9$; Table 2: the amount of strain was measured from the deflection of vertical markers on the steel jacket (see Laumonier et al., submitted): whenever wrinkles appeared onto the jacket, the measurement of the angle of deflection was made over lengths several times the wavelength of wrinkles). Then, tangential sections [xz] normal to the plane of shear and with x parallel to the direction of shear were cut from the sample where the strain is maximum, and embedded in epoxy for observation and chemical analyses. However, when the sample and jacket displayed wrinkles (the toothpaste texture of Barnhoorn et al., 2005; see below), tangential sections were cut inward relative to the jacket waves, so as to minimise their influence, with a corresponding lower local strain (Paterson and Olgaard, 2000). Additional details on the

experimental set-up and techniques can be found in Paterson & Olgaard (2000). The torsion of two conjugate half cylinders (one mafic and one felsic sharing a vertical interface) was also tested during the preliminary stages of this work at run temperatures of 1170 and 1200°C, at which both compositions have similar viscosities (Laumonier et al., in preparation), the viscosity of the felsic layer being slightly lower than that of the basalt. However, that geometry led to the near immediate tilt of-axis of the entire column as soon as deformation was applied, which forced us to stop experiments to avoid serious damage of the entire apparatus. Hence, although appealing, such an assembly proved impractical for textural and rheological analyses in the context of magma mixing, and it was not explored further. These experiments do not reproduce natural cases, so they are not presented here.

Static experiments with the same geometry were performed for 3 and 50 hours at 300 MPa and 1170°C, to document textural and chemical changes occurring without applied deformation. The 3 hours experiment was drop quenched so as to preserve as much as possible the chemical and textural state reached by the samples loaded into the Paterson press prior to deformation. The 50 h experiment, though not drop quenched, yields information on the system as it proceeds toward equilibrium.

3. RESULTS

3.1. Static conditions

3.1.1. 3-hour static, drop quenched run

In the 3-hour drop quenched run at 1170°C, the whole geometry of the stack was preserved at low magnification (Fig. 4A). In detail, changes in layer thicknesses, of the mafic end-member in particular, occurred (ρ_1 : -1.2%; β_2 : +7.3%; ρ_3 : -2.7%; β_4 : +5%). The residual crystals (46 % in volume) of the mafic component are plagioclase, olivine phenocrysts and microcrysts and rare clinopyroxenes. All phases, in particular olivine, display strong resorption textures. The plagioclase rims have almost fully disappeared and the touching crystal framework is hardly visible, though

plagioclase crystals display a SPO (Fig. 4B). The β_4 layer exhibits a regular subvertical SPO as in the starting basalt, the fabric intensity being similar (2.17) to the starting one. The SPO in the β_2 layer is more irregular, with several main orientations of the long axis of local ellipsoids (i.e. at $\sim 15^\circ$, $\sim 85^\circ$ and $\sim 135^\circ$), and an overall lower fabric intensity (1.24). The plagioclase microphenocryst cores display a size distribution and a chemical composition similar to the one in the starting basalt (Fig.SI 1, 5A).

The outer edges of mafic disks are recognizable by the surface defined by microphenocrysts cut sharp during disk preparation (Fig. 4C) and preserved after the experiment. However, in between haplotonalite and basalt disks, reaction zones have developed, with various textural features depending on whether the upper or lower contact is observed. Where the haplotonalite overlies the basalt (contacts ρ_1 - β_2 and ρ_3 - β_4) two layers develop. The one close to the haplotonalite, termed crystal-bearing layer (c-b layer, Fig 4C), is composed of intermediate plagioclases (An₃₄ to An₆₅) set in a chemically zoned melt (c-b layer, Fig. 5E; Table 3) which broadly defines a trend between the felsic end-member and the average composition of the mafic melt at 1170°C (“pocket”, Fig. 5E, only melt pools without quench phases were analysed). In contrast, close to the basalt, the layer is almost free of crystals (c-f layer) and displays a variation in thickness (from ~ 0 to 200 μm) with local mafic plumes intruding the felsic layer (Fig. 4C). The β_2 - ρ_3 contact exhibits roughly the same features except that no large mafic protrusions into the felsic component are observed, and the crystal-free layer (c-f) is thinner when it exists. Aside from these textures at the edges of the disks, the inner part of the mafic layers exhibits an homogeneous crystal distribution and melt composition, as revealed by the MgO concentration which varies by less than 1 wt.% for SiO₂ ranging from 51 to 53 wt.% (“melt β ” in Table 3, Fig. 5E). Some melt compositions depart slightly from those produced at longer run durations and drop quenched (compare black triangles and stars in Fig. 5E), reflecting the lower melt fraction in the 3 h run. Pyroxene has a Mg# = 75-83 (molar MgO/(MgO+FeO_{tot}) ratio), slightly lower than in the starting material (Fig. 5B). In contrast, olivine crystals have a range of Mg# (Fig. 5D; Table 3): cores of

phenocrysts are similar to starting one whilst their rims have a high Mg# (~85). Newly grown (euhedral) olivines have also a high Mg# (>83), whereas some phenocrysts are almost completely resorbed and have an intermediate Mg#~80 (Fig. 5D, Fig.SI 2). Euhedral olivines were observed only within the mafic layers.

In the haplotonalite layers, a ~120µm thick sodic-plagioclase halo is regularly distributed along their edges (Fig. 4C,D & E). Plagioclases are too small to be analyzed individually. However, the felsic crystals + melt mixture has an homogeneous anorthite content (An19), similar to the felsic glass, suggesting limited contamination, if any, by the mafic component. Crystal orientation and distribution suggest heterogeneous nucleation and subsequent growth, either from the mafic layers or along the capsule walls (Fig. 4E). As stressed above, this plagioclase layer is locally intruded by small melt plumes growing from both sides of the mafic layer (Fig. 4C, D).

3.1.2. 50-hour static run

In the 50 hour static run, the whole geometry of the stack was preserved as well (Fig. 4F). However, slight changes in the layer thickness are also apparent. The mafic disk thickness increased by roughly 9 (β2) to 7% (β4) whereas that of the felsic disks decreased by about 5 (ρ1) and 3 % (ρ3). The overall sample length increased by ~2.5 % as measured on the section presented in figure 4F. No measurable variation of the sample diameter occurred during the experiment.

The mafic end-member is composed of microphenocrysts of plagioclase, clinopyroxene, olivine and a mixture of melt and quench crystals; no oxides are visible any more (Fig. 4H). In contrast to the drop quenched experiment, the melt is difficult to analyze because of the abundance of quench crystals. Plagioclase exhibits the same network organization as in the partial melting test conducted at 1170°C (Fig. 4B & G). Plagioclases display a regular SPO as in the starting Santorini basalt. As in the 3-hour experiment, the fabric intensity is either close (2.13, β4 layer) or lower (1.59, layer β2) than in the starting material. The plagioclase size distribution is broadly preserved (Fig.SI 1) with an average plagioclase core shape ratio ~2.8. Almost all plagioclases are zoned, displaying a near continuous rim of Na-rich overgrowth (Fig. 4I). They represent roughly the same

phase proportions in both β_2 (49%, cores = 31% + rims = 18%) and β_4 (52%, cores = 33% + rims = 19%) layers. The composition of the plagioclase cores in the static experiment (An78) is again close to that of Santorini basalt (Fig. 5A; Table 4). Plagioclase rim within the mafic layers varies from An47 to An67. Clinopyroxene and olivine crystals of roughly 50-100 μm size and quench crystals, both with composition similar to that of the starting material and the 3h static experiment (Fig. 5B; Table 4).

As in the 3h static experiment, reaction zones developed between end-members. The upper haplotonalitic disk (ρ_1) is separated from the basaltic disk (β_2) by two layers (Fig. 4H). A lower layer, (crystal-free layer, c-f, Fig 4H), extends up to $\sim 80 \mu\text{m}$ and is composed of melt and rare plagioclases (Table 4). The upper layer (crystal-bearing layer, c-b, Fig 4H), is about $\sim 150 \mu\text{m}$ thick, and contains small plagioclases (40% of the layer) in an intermediate grey level melt (Fig.4H). The average size of the long axis of these plagioclases is $6 \mu\text{m}$, much smaller than plagioclases in the starting basalt (Fig.SI 1). They are strongly oriented perpendicularly to the interface and are slightly larger towards the mafic disk. Single grain composition ranges from An29 to An72, and the general small crystal size makes it difficult to document any intragrain variation (Fig. 5A, Table 4). The melt in the crystal-bearing layer has a SiO_2 content between 57 and 68 wt.% (Fig. 5E), while in the crystal-free layer the melt is more homogeneous with SiO_2 between 55 and 58 wt.% (Fig. 5E). The two contacts between the lower disks (β_2 - ρ_3 and ρ_3 - β_4) display only a crystal-bearing layer (Fig. 4I). However, locally, the top of the lower mafic disk displays melt pockets or lenses $300 \mu\text{m}$ thick and several hundreds of μm across (Fig. 4I). The transition from these lenses to the mafic disk is short. The melt displays local heterogeneities such as rolling up structures on SEM images (black arrow, Fig. 4I) and variable MgO contents (from ~ 3.5 to 8.3 wt.%, “pocket” in Fig. 5E). No melt analysis with SiO_2 content lower than $\sim 54\%$ was obtained in the 50 h run. This gap is however filled by the melt within the mafic layer (β layer) of the 3 h static experiment, suggesting that the more mafic melt in the longest static experiment produced clinopyroxene/plagioclase small quench crystals (Fig. 4I).

The variations of melt SiO₂, FeO, MgO, and Na₂O contents across the felsic/mafic contact zone (Fig. 4I) are shown in [figure 6](#), from -60 μm (mafic side) to 90 μm (felsic side). The chemical zoning is illustrated with several traverses either in the melt lens (profiles A and B, Fig. 4I) or above it where abundant plagioclase microphenocrysts crystallized (profiles C, D and E, Fig. 4I). The traverse B displays “anomalies” close to the plagioclase phenocrysts. Indeed, the FeO and the CaO contents are ~2 wt. % higher and ~0.5 wt. % lower close to the plagioclases. Analysis closer to the haplotonalite was not possible due to the abundance of small plagioclases. Despite heterogeneities imparting local zig-zag patterns (in particular towards the mafic end-member, [Fig. 6](#)), all traverses define a single common trend bridging the two end-members, as expected.

3.2. Dynamic conditions

3.2.1. Textures

All torsion experiments conducted in the temperature range 1170-1200°C produced mingling/mixing textures such as enclaves (in the sense of aggregates of mafic minerals inside the felsic component), mafic melt filaments carrying some crystals, and isolated crystals. No influence of the layer initial thickness, strain rate within the range of our experimental conditions was noticed. In contrast, experiments conducted at lower temperatures (900 to 1160°C) did not produce any such textures, as illustrated by the run performed at 1160°C, which will be presented for comparison. The [figure 7](#) shows the texture of the iron jackets moulding the samples after torsion. Strain distribution is roughly homogeneous for all experiments conducted at temperatures higher than 1160°C, whereas experiments at equal or lower temperatures display a heterogeneously distributed strain ([Fig. 7A](#)) with the mafic layer being weakly deformed ($\gamma_{\text{local}} = 0.5$), almost all the strain being accommodated by the felsic layer ($\gamma_{\text{local}} > 10$). The calculated strain at the interface between both end-members ($\gamma_{\text{local}} = 2.9$) is comparable to the bulk strain of other experiments. The strain distribution is closely linked to heterogeneities in viscosity. At temperatures $\leq 1160^\circ\text{C}$, the

viscosity of the mafic layer is higher than the one of the felsic magma which hence preferentially accommodates the strain (Laumonier et al., in preparation).

Tangential [xz] sections were cut from the deformed samples to carry out textural analyses on SEM images (Fig. 8). Local strain was quantified from the radius and length of the sample, and the twisting angle (Paterson & Olgaard, 2000). Despite a local strain $\gamma_{\text{local}} = 4.3$, the 1160°C run shows no physical interactions between end-members, whose interface contact remains sharp and flat (Fig. 8A, only the lower part of the sample is shown). Plagioclases in the β_2 mafic layer display two main fabrics: a vertical one against the alumina lower piston at the bottom part of the section, and a tilted ($\sim 35^\circ$) to horizontal one when approaching the felsic layer ρ_1 . As can be seen by comparing Figures 8A and 7A, the upper SPO is concordant with the strain distribution through the mafic layer. The bulk fabric intensity has not increased (1.28), however, as compared to the starting one (Section 2.2.1, Fig. 4B,G).

In contrast to the 1160°C run, all experiments conducted at higher temperatures (1170°C-1200°C) show macroscopic interactions between both materials (Fig. 8). Even at relatively low deformation ($\gamma_{\text{local}}=2.6$), some basaltic disks disaggregate and the initial cylindrical shape with a planar contact parallel to the direction of bulk simple shear is not recognizable anymore (Fig. 8B to J). The mafic to felsic interface becomes a lobate contact, lobes having a space and size distribution of about $\sim 400 \mu\text{m}$ (Fig. 8I). Many mafic (Fig. 8B, C, G, H, I, J) and felsic (Fig. 8B to G, I, J) “gulfs” were created, at different distances from the sample outer edges. Mafic layers having retained their flat lying shape display a relatively homogeneous and vertically oriented SPO, reminiscent of that of the starting material (β_2 in PP157a and PP160c, and both mafic layers on the PP157b section; Fig. 8). In contrast, disrupted mafic layers of experiments conducted at 1170 and 1200°C have complex SPO patterns such as the β_4 layers in PP157a, PP160b, PP161a, PP164b, PP176b and β_2 layers in PP160b, f, PP164a, b and PP176a (Fig. 8), sometimes with pronounced SPO deflections parallel to the sense of shear (ex: β_4 layers in Fig. 8G). Although SPO and rose diagram distributions are different from those of the starting material, no obvious relationships

between fabric intensity and either finite strain or strain rate emerge (Fig. SI 3). In some cases (Fig. 8F, G, J), the SPO increases, oriented at an angle of ~ 45 to 75° relative to the shear plane, with a fabric intensity (from 2.1 to 3.2) higher than in the starting material (1.2-2), but the reverse is also seen (Fig. 8H), corresponding to values of SPO lower than 1 in figure SI 3.

Enclaves

As the lobes stretch out they end up as enclaves of mafic material within the felsic host (Fig. 8B, J, 9A, B). The enclave paragenesis (plagioclases, pyroxenes, melt and rare olivines) and the textural arrangement of crystals remain similar to that of the parent mafic layers. The size of enclaves typically ranges between 300 and 500 μm in length, with irregular and angular shapes defined by the largest microphenocryst of plagioclases (Fig. 9B). Plagioclases with 5-15 μm length occur either within true enclaves or within those still connected to the mafic disk. These small plagioclases have a size and aspect ratio similar to those in the crystal-bearing layer of the static experiments. Rare felsic enclaves were observed in the mafic end-member (Fig. 8C, 9C). Most of the time, felsic embayments remain linked to the main parts of the haplotonalite.

Stretched inclusions or melt filaments

Mafic melt filaments in the felsic component are observed in the highest strain rate experiments ($\dot{\gamma} \sim 10^{-3} \text{ s}^{-1}$, PP160 and PP176; Fig. 8F, J, 9D, E), keeping in mind that given strain rates are average values, and local variation of the strain rates are probable yet not possible to determine. Such melt filaments may carry a few microphenocrysts of plagioclase and rare pyroxenes, and are devoid of profuse quench textures having only rare tiny quench-like crystals (Fig. 9D). This suggests that the melt filaments have a broadly well preserved composition. They extend up to 4.5 mm length and are always less than 100 μm thick. Most filaments are planar while few are irregular. All are connected to the main mafic layer by a thin film of melt. Plagioclase and rare pyroxene crystals issued from the basalt are both carried by filaments. As long as they are located

within the filament, they tend to follow melt motions. Plagioclase shows textures similar to those present in the c-f layer discussed in the static experiments (compare Figs 4I & 9D). In addition, homogeneous small acicular plagioclases are common in the filaments. They are abundant when the contact between the filament and the felsic host is progressive (white arrow, Fig. 9E). Both their morphology and spatial distribution are reminiscent of the plagioclase population of the crystal-bearing layer observed in the static experiment (Fig. 4H, J, 9E). Pyroxene from the basalt is rare, and no newly grown pyroxene has been detected in the filaments. Olivine crystals are also absent in the filaments.

Isolated crystals

Plagioclase and pyroxene crystals originated from the main mafic layers are observed as isolated grains in the felsic component (Fig. 9F). They are sometimes present around enclaves, suggesting local enclave disaggregation. In contrast, they are abundant in felsic embayments formed at the felsic to mafic main contact (Fig. 8B, D, H, J, Fig. 9F). Some of the isolated pyroxenes are zoned, displaying a darker rim while others are non-zoned. The population of isolated plagioclase is smaller in size than the plagioclase populations in the mafic layers in torsion and static experiments and from the Santorini starting basalt (Fig. SI 1).

3.2.2. Composition of minerals and melts

The selection of minerals/glasses to be analyzed was done considering the local textures. Glass analyses were performed in the zone of interaction between two starting end-members and along the contact between crystals and melt. Representative analyses are shown in Table 5.

Minerals

In all experiments, pre-existing crystals coexist with a variety of newly grown phases, essentially plagioclase, pyroxene and some olivine. There are no obvious textural or chemical differences between plagioclase populations produced in either static or dynamic runs. Figure 5A shows the

range of plagioclase compositions obtained in all the run products classified according to their origin. It can be seen that the experiments produced an almost continuous range of plagioclase composition, from An81 down to An29, the latter being similar to the An30 determined by [Picard \(2009\)](#) for the haplotonalite alone. Core compositions of large plagioclases in dynamic experiments are similar to that of plagioclase cores in both the starting rock and static experiments (~An72 to ~An81). In both types of experiments, rim compositions of large plagioclase extend down to An47-48, which is similar to the lowest An content of the plagioclase rims of the starting material (An48), suggesting on-going re-equilibration of plagioclase outer border (either via diffusion or more likely by local growth). Isolated large plagioclases found in the dynamic experiments have again compositions similar (An77) to those of the core plagioclases in the starting basalt. Lastly, the An content of plagioclase growing in the reaction zone of the 3h and 50-hour static experiments can be as low as An38, clearly trending toward the plagioclase in the haplotonalite end member.

Clinopyroxene composition also varies considerably, as illustrated by its Mg# on [Figure 5C](#). As for plagioclase, clinopyroxene cores of static and torsion experiments are similar to those in the starting basalt with a Mg# ranging between 73 and 83 ([Table 5](#)). Clinopyroxenes present within melt filaments and enclaves are all the more similar to those of the static experiments, suggesting an origin by entrainment from the main mafic layer rather than by local growth. In contrast, clinopyroxenes with higher Mg# (85 to 88) can be found either as rims on pre-existing and isolated large pyroxene crystals or on isolated non zoned crystals, both included in the haplotonalite. Considering the slow kinetics of solid state diffusion as compared to crystallization rates (which differ by orders of magnitude), and the short run duration, these pyroxenes rims most probably represent the new crystallization of high-Mg# pyroxene. It has to be noted that, unlike the case for plagioclase, there is a difference between newly grown clinopyroxenes in the static and dynamic experiments, those produced under static conditions being compositionally less diverse than the group produced under deformation, the latter clustering also at higher Mg#, around 87 ([Fig. 5B](#), [Table 5](#)). Olivine composition issued from torsion experiments reproduces the behaviour described

in static runs: cores of phenocrysts have Mg# ranging between 73 and 78, close to the same population in both static runs and starting material. Smaller olivines, either resorbed or euhedral crystals, have higher Mg#, (80 to 86). Phenocrysts are present both within the mafic layer and close to the contact with the felsic melt, whereas the newly grown crystals were only observed relatively far from the felsic layers.

Glass

Glass analyses were performed in areas free of quench crystals to facilitate interpretation. All analyses performed within interaction zones exhibit a near continuous range of compositions between a pure haplotonalitic composition ($\text{SiO}_2 \sim 69$ wt. %) and mafic glass obtained in the static partial melting experiments with basalt ($\text{SiO}_2 \sim 52$ wt. %, stars on Fig. 5E, Table 5).

As illustrated in the SiO_2 vs. MgO diagram (Fig. 5F), the glass compositions at the contact zone in torsion experiments range between haplotonalite to heterogeneous compositions broadly trending towards the mafic end-member ($3.5 < \text{MgO} < 7.2$ wt.% for $\text{SiO}_2 \sim 55$ wt.%). Glasses from filaments have a composition clearly different from that of the partial melting experiments with basalt only (stars, Fig. 5E & F). The composition of filaments is relatively clustered and falls within the fields defined by the “crystal-free melt layer” or “melt pocket” documented in the static experiments (layer c-f on Fig. 4H & J). In detail, mapping of FeO, CaO & MgO concentration illustrates the correspondence between the filament and the main mafic layer (Fig. 10). The inner parts of glass from filaments have SiO_2 contents ranging from 55 to 59 wt. % (Fig. 5F). The most stretched and thinnest parts are those most depleted in iron and magnesium. From the central parts of filaments toward the felsic host, the transition can be either progressive or sharp (Fig. 10): for instance the CaO gradient is more than 10 times higher in a filament in PP160 (0.70 %/ μm , Fig. 9D, 11A) as compared to a filament in PP176 (0.06 %/ μm , Fig. 9E, 11A). The glass inside the enclaves is relatively evolved, with SiO_2 concentrations higher than 58 wt.%, and an MgO content slightly higher than the mixing line between both end-member, though still close to the composition of the glass in the mafic static experiments.

3.2.3. Crystal-melt relationships

Deformation brings about various crystals issued from the mafic component (Fig. 8 & 9) into the felsic layer. Transects have been performed from the pure haplotonalitic melt towards (1) crystals in enclaves and (2) isolated crystals.

The transition between a plagioclase from an enclave and the surrounding felsic melt is progressive (Fig. 9b & 11B) suggesting the presence of intermediate melt surrounding the crystals in the enclave. Conversely, isolated plagioclases display a sharp contact with the felsic host, with no detectable intermediate melt (Fig. 9F & 11B). Such isolated plagioclases (An78) have irregular contours suggesting on-going resorption. As mentioned previously, most of the isolated pyroxenes (augite) have a core similar to the pyroxene of the main mafic component but display a rim (Fig. 9F) with a higher Mg# (>85, Fig. 5B). No chemical gradient could be found in the melt around isolated pyroxenes or plagioclases.

4. DISCUSSION

4.1. General considerations

We first note that various studies have emphasized the fundamental invariant-scale nature (or fractal) of mixing processes (e.g., De Campos et al., 2011; Perugini et al., 2012), which implies that conclusions drawn from observations at micrometric scales may apply to higher scales as well. Mixing may arise from a generally crystal-poor mafic magma intruding a more viscous felsic host, though replenishment of a reservoir by a more felsic magma does occur as well (e.g., Eichelberger & Izbekov, 2000 and references therein). The temperature range investigated in our experiments was imposed by the melting interval of the basalt. We stress however that the applied temperatures are close to those expected in nature in volatiles-poor systems, and whenever the mass of mafic magma is sufficiently large to locally maintain elevated temperatures. Our system is thus comparable to some natural environments in terms of chemical and rheological contrasts, the latter being governed by the temperature at which deformation was applied (Fig. 1). Clearly, however,

magma mixing is mostly documented in H₂O-rich systems, but our aim here is to provide a comparative basis for mixing experiments performed with added water (Laumonier et al., submitted).

The geometry of the sample coupled with the torsion deformation simulates flow conditions commonly observed in nature such as on the borders of dykes replenishing magmatic chambers (e.g., Petford, 1996). Yet, the simple shear applied in our experiments is clearly much lower (10-100 times, see De Rosa et al. 1996) than that prevailing in a reservoir during replenishment, during convection, or during transfer in a volcanic conduit, and so is the deformation reached in our experiments. However, although the bulk strain accessible with our experimental set up and apparatus is relatively limited ($2.0 < \gamma_{\text{bulk}} < 3.9$, locally larger), it produced a variety of mixing textures similar to those documented in many volcanic or plutonic rocks, as discussed below. We re-emphasize that textures created in our torsion experiments likely record the incipient stages of mafic-felsic interaction processes when the shearing deformation is parallel to the interface. Other geometrical relationships, though undoubtedly of interest and geologically relevant, have not been successfully tested for the moment.

Below, we first discuss the mechanisms of formation of the different interaction zones produced in the static experiments, which define the starting point of the system before deformation was applied. We then explore in detail mixing/mingling textures. Finally, we compare our mixing experiments with previous descriptions of natural and experimental studies of magma mixing.

4.2. Development of the interaction zone

Static experiments show that despite a density 15% higher, the basaltic β_2 remains locked between the felsic layers over the time scale of our experiments (Fig. 4A, F). They also show that an interaction zone between end-members develops, which thickness increases with time, as found in previous similar studies at 1-bar (e.g., Kouchi & Sunagawa, 1982; 1985). As anticipated, the composition of melts within this interaction zone is intermediate and clearly reflects the effects of

cross contamination which is driven by chemical diffusion (ie, Watson, 1982). Application of diffusivity laws available for the main melt components of interest shows that at 1170°C, self diffusivities range from 10^{-12} - 10^{-15} cm²/s (Si) to 10^{-11} - 10^{-14} cm²/s (Al, Mg, Ca) up to 10^{-9} cm²/s (Na, K), which correspond to diffusion distances (calculated for 1 hour and using the relationships $x = (Dt)^{1/2}$, x being distance (m), D diffusivity (cm²/s), and t time (s)) of 1-30 microns (Si), 10-200 microns (Al, Mg, Ca) and 400-2000 microns (K, Na), respectively. The latter value is in line with the high mobility of alkalis in silicate melts or glasses. However, the few experimental data available on a multicomponent diffusive system (e.g., Watson, 1982), such as in the present interaction zone, show that alkali diffusivities, in particular Na, decrease by up to three order of magnitude (relative to self diffusivity values), being comparable to those of Ca, Mg or Al (ie 10^{-12} - 10^{-13} m²/s see Fig 3, 4 of Zhang et al., 2010). The calculated thickness of diffusion for the latter elements extends up to 200 microns, being comparable to the observed thickness of the reaction zone, which may have therefore originated in part from diffusion, in particular during the static stage prior to deformation. The fact that the interaction zone has size and chemical characteristics comparable to those anticipated from static diffusion models, shows that deformation has per se no intrinsic effect on material transport properties (ie element diffusion or viscosity, see Laumonier et al., in preparation), in the range investigated here. Beside diffusion, the variability in melt compositions (Fig. 5E) also reflects possible convective motion effects of the melt and the interplay between the kinetics of melting and crystallisation of minerals (see Zhang et al., 1989), which affect diffusion profiles by changing the local melt composition. That the interaction zone develops, although not symmetrically, on the top and bottom parts of the β_2 layer (Fig. 4 C, D) is supportive of a diffusion process and shows that such a zone is unlikely to result from a density-driven process. Other mechanisms, such as a local pressure increase upon a positive change in volume during melting (Lange and Carmichael, 1990), may have played a role, however, though they are difficult to quantify. Although the lower thickness, or even absence, of the c-f melt zone at the lower interface of β_2 layer may suggest at first sight that melt segregation atop a compacting partially

melted layer (McKenzie, 1984) occurred to some extent, there are no clear evidence of crystal accumulation/concentration across basaltic layers. The generally weaker fabrics of β_2 layers, as compared to those of β_4 , indicates of a higher mobility of the network, perhaps reflecting that β_2 is sandwiched by 2 mobile layers (ρ_1 and ρ_3).

As the interaction between the c-f layer (Fig. 4C, H) and the felsic component proceeds, new sodic plagioclases crystallize, forming the crystal-bearing layer (c-b layer, Fig. 4H). Plumes and melt pockets (Fig. 4C, E, J) could result from higher local melt fractions, mirroring local heterogeneities of the starting modal composition of the basalt (e.g. higher fraction of olivine and/or pyroxene). Altogether we surmise that the c-f melt layer results from a combination of factors, which include advective and diffusive processes namely, (1) melt migration from inside the mafic layer and (2) progressive contamination of it by the surrounding more felsic melt via chemical diffusion. Quite remarkably, this layer displays a relatively homogeneous composition, clustering midway between the two end-members. Under the explored P-T-duration conditions, the interaction zone thickness is generally on the order of 100-200 microns (Fig. 4), which corresponds to less than 10% of the β_2 layer thickness. As we shall see below, it is this level (and the crystal-bearing one) that supplies the bulk of material for mixing during deformation. It is worth to note that the melt of the crystal-bearing layer is more differentiated than the one in the crystal-free layer (Fig. 5E).

An unexpected feature of our experiments was the growth of a plagioclase-rich zone at the haplotonalite/capsule and haplotonalite/basalt interfaces at temperatures higher than 1150°C. This zone is also present in drop-quenched experiments, showing that it is not a quench phenomenon. Rather, it results from heterogeneous growth of plagioclase which occurs everywhere along the interfaces of the felsic magma. It ends up forming a more rigid layer surrounding the mafic magma, which obviously affects interaction processes. From the rheological viewpoint, however, it can be considered that such a rind mimics a quench border of a mafic intrusion. As this zone progressively develops during the experiments (compare thicknesses between 3 and 50 h durations on Fig. 4), it is also a chronological marker for mafic magma motions; mafic pieces of magma with a well

developed halo of sodic plagioclase may represent portions of such a mafic layer entrained early in the deformation sequence, whereas enclaves without such a halo may have been formed during the last stages of the experiment. However, we stress that the development of such a rim is specific to our experimental conditions and set-up, as well as to the chemical gradient between end-members. Hence, direct application of our experimental findings to natural contexts should be made keeping this in mind.

4.3. Sequence of enclave formation and disruption

Our experiments reveal that the rheological response of the basaltic layer to shear deformation changes abruptly in a narrow temperature interval, specifically between 1160°C and 1170°C, within which the crystal fraction decreases from 64% down to 46% (Fig. 2A). Previous rheological measurements have indeed revealed that the threshold between solid to liquid-like behaviour in partially molten systems lies in the interval 30 to 60 % in volume (e.g., Arzi, 1978; Van der Molen and Paterson, 1979; Vigneresse et al., 1996; Rosenberg & Handy, 2005; Caricchi et al., 2008; Picard, 2009; Picard et al., 2011), the exact value depending, inter alia, on particle aspect ratio. Picard et al (2011) measured a critical crystal fraction of ~30%, for a suspension composed of plagioclases with an aspect ratio of 5. The shape ratio of plagioclases in our experiments is ~3, making them less prone to sustain a rigid network compared to higher aspect ratio crystals. For instance, Philpotts et al. (1998) experimentally demonstrated that a non deformed suspension with as little as 25% crystal with an average shape ratio of 5 remains rigid, which they concluded is due to the existence of a 3D framework (see also Martin et al., 2006a).

Based on our experimental findings as well as on previous work, we hypothesise three general regimes during mafic-felsic magma interaction, depending on whether the crystal network of the mafic layer is rigid, strain breakable or absent (Fig. 12).

Magmas with rigid crystal network: In the case of a high crystal fraction ($\Phi_s > \sim 50\%$) a rigid crystal network exists and, neither mingling nor mixing occur, such as in all experiments conducted up to 1160°C, (Fig. 8A & Fig. 12A). Under these conditions, crystals form a framework strong

enough to preserve mafic layers from disruption and the deformation is accommodated by the less viscous felsic magma (Fig. 7A).

Magmas with breakable crystal network: Magmas with a lower crystal fraction ($\Phi_s < \sim 50\%$) are likely to deform and mix (Fig. 12B, C). Two behaviours can be depicted according to the absence of a touching crystal network ($\Phi_s < 25\%$) or the presence of such a network, but still strain breakable ($25 < \Phi_s < \sim 50\%$), as in all of our experiments at 1170 and 1200°C. In both case, the mingling process may be initiated after interface irregularities are created, possibly due to crystal framework deformation or melt segregation.

In the case of a breakable crystal network (Fig. 12B), the application of strain allows the development of a new fabric which may partly overprint the original one. In general, however, both enclaves and mafic layers do not show a pronounced increase in fabric intensity (max 3.17, Fig. 8G) relative to starting values (1.9, Fig. 2A), suggesting that disruption and reorganisation of the crystal network remain limited. Also the geometry of the fabric is not always consistent with that of deformation (Fig. 8H). In contrast to this seemingly near constancy of fabric parameters, the mafic to felsic interface displays more spectacular modifications. In particular, when a certain amount of strain is applied (of about $\gamma_{\text{bulk}}=3$, see Table 2), the interface becomes irregular and evolves rapidly into lobes (Fig. 8I, 12B-1 & -2). As strain increases, the lobes separate from the main mafic layer owing to local break-up of crystal network, yielding enclaves (Fig. 12B-3). The crystal network maintains the enclave as a self-consistent parcel of magma and inhibits its immediate disintegration (Fig. 12B-5). At larger strains, enclaves may have two ways to be preserved: either from an intrinsic resistance arising from the persistence of a rigid crystal network ($>50\%$), or from an extrinsic strengthening owing to the presence of a rigid quenched outer rim (Fig. 12B-5 to -9). If the host magma is less viscous than the crystallized enclave, then the latter may be preserved, whatever strain is applied. The enclaves we produced in our experiments are generally well preserved due to their relatively large crystal fraction. However, it is probable that they would have not survived at higher strain. In the case of a cold reservoir being replenished, quench margins may develop on

mafic forerunners and such a freezing mechanism is usually thought as one allowing enclave preservation (e.g. Pin et al., 1990; Barbey et al., 2008), but volatile exsolution may overcome this factor (Martin et al., 2006a). As stressed above, although true quench margins cannot be produced in our experiments, the plagioclase-bearing layer resulting from heterogeneous nucleation of the haplotonalite end member acts a rigid outer lid, damping to some extent enclave deformation. Crystal-poor ($\Phi_s < 50\%$) enclaves may dislocate, generating schlierens at high shear strains, until they completely disaggregate resulting in isolated crystals dispersed in the host (Fig. 12B-4 to -8).

Magma without crystal network: This is a regime more specifically investigated by previous experimental studies, that is, one in which the melt phase exerts the dominant role on magma rheology (e.g., De Campos et al., 2011; Morgavi et al., 2012). Our experiments did not explore temperatures high enough to produce crystal-free suspensions, though such a regime has occurred in some part of the samples, owing to higher melt fractions being locally reached, such as in melt pockets or in the crystal-free layer of the interaction zone. Figure 12C illustrates the behaviour expected to happen in such a case, which is obviously the most favourable to efficient mixing (see again De Campos et al., 2011). Filaments represent the typical scenario where few crystals compose the mafic end-member; only plagioclases are carried by filaments due to the early melting of both olivine and pyroxene crystals (Fig. 12C-1&-2). Once interface heterogeneities are created (rolling up of a phenocryst, melt fingering due to injection (Perugini & Poli, 2005), change in the deformation geometry according to the interface...), protracted deformation is likely to produce stretched structures, layering, ending up into a hybrid magma if the process is allowed to proceed to completion (Fig. 12C-3 to -6).

4.4. Fabrics

Measuring the fabric of enclaves is a common way to determine the regime or intensity of the deformation that affected the magma mixture during mixing (e.g., Paterson et al., 2004; Perugini et al., 2004; Caricchi et al., 2012). Our experiments shed light on some important aspects on the likely timing of magma fabric acquisition. They first clearly show that when a contrast in viscosity

exists, only the less viscous member is being deformed, and that the imprint of deformation on the more viscous one is almost null (when the more viscous material has a near solid behaviour). In all experiments performed in the temperature range 900-1160°C, the fabric of the mafic layers does not show any obvious change in either its orientation or intensity, except close to the contact between end-members in the 1160°C experiment (Fig. 8A). This is again related to the existence of a strong rigid mineral network of the mafic end-member under the explored conditions, resulting in a large viscosity contrast between end-members (Fig. 3). Quite surprisingly, however, the same could be said when deformation conditions are close to, or beyond, the threshold for mafic magma disruption discussed above (melt fraction > 50%). Indeed, despite its decrease in strength, the mafic material does not record in any systematic way the parameters of the applied deformation. Rather, this threshold is above all characterised by the abrupt start of mafic enclave formation. Hence, the experiments confirm the conclusion reached by Scaillet et al. (2000), using phase relationships arguments, that enclave fabrics record dominantly, if not exclusively, magma deformation prevailing at near solidus conditions, during which the viscosity contrast is low, but also the strengths of both materials are high, owing to their high degree of crystallisation.

4.5. Chemical effects

The experiments produced a range of compositions, solids or liquid, which broadly form linear trends between the two starting end- members (see also Kouchi and Sunagawa, 1982 for comparable findings using a similar set-up and conditions (except pressure and strain rate)). Deviation from linearity is most easily accounted for by local heterogeneities arising from either crystallisation or melting effects, and from the vagaries of quench-related effects. One remarkable feature is that, despite the short durations of our experiments, a near complete range of plagioclase compositions was obtained, as a result of plagioclase being stable in both magmas (Fig. 4, 5A, 9). Both crystal melting and growth occur simultaneously, as evidenced by resorption features affecting all minerals and the growth of new plagioclase, pyroxene, and olivine. Hence melt inclusion formation during mixing may preserve a wide range of liquid compositions.

The static drop quenched experiment shows that olivine with $Mg\# = 75$ is not stable under our experimental conditions. Instead, a rim and new euhedral olivine develop characterized by a higher $Mg\#$ (~85; Fig. 5D). The absence of olivine close to the felsic layers indicates that it is stable in the most mafic parts only. Some high $Mg\#$ (85) pyroxenes were found in similar static experiments, though not presented here. They are located in an intermediate layer, close to the felsic layer, atop an olivine phenocryst. One explanation for the occurrence of such high $Mg\#$ pyroxene and the ones in torsion experiments is that they crystallized from a melt enriched in MgO owing perhaps to locally enhanced olivine melting. Another possibility is that pyroxene grew out of equilibrium producing anomalous, Mg-rich, compositions. In both cases the intriguing observation is that such high- $Mg\#$ pyroxenes have been detected mostly as embedded in the haplotonalitic magma, notably in felsic embayments located at the sample periphery where the strain and strain rate are the highest. The overall process must be indeed relatively fast as few sodic plagioclases crystallized in the embayments and isolated pyroxenes do not had sufficient time to equilibrate with the enclosing haplotonalite, perhaps owing also to the lack of nutrients in the newly surrounding melt (i.e. Fe, Mg). We suggest that this could reflect a sort of chemical quenching.

An important observation of the present study is that, under the investigated conditions, there is no melt coming from the interior or basalt layer being directly ejected into the felsic magma. Indeed, melts produced in the partial melting experiments or in the interior of the mafic layer, are both considerably more mafic than any filament, thin or thick (Fig. 5F). Filament compositions are very similar to melts analysed in the interaction zone of static experiments (Fig. 5E). This chemical argument along with textural features given above, suggest that filaments are most likely stretched remnants of crystal-free/bearing layers or melt pocket documented in the static experiments (c-f and c-b layers; Fig. 12C-1, -2). The interaction zone appears thus to be preferentially mobilized during deformation, possibly due to a lower crystal fraction, together with some plagioclase phenocrysts and, more rarely, pyroxenes, from the immediate underlying basalt. In detail, the interface between the filament and its host may be compositionally either sharp or

progressive (Fig. 9D, E) depending on the relative rates of diffusion and strain, as well as elapsed time. An interface is progressive when the diffusion overprints the contacts moulded by deformation (Fig. 4 & 9E). In contrast, a sharp contact occurs when chemical diffusion cannot operate due to fast magma motion, or if the intruding magma is chilled. The stretched inclusion shown in figure 9D (profile G) illustrates this feature: it is free of sodic plagioclase halo whereas the surrounding connected larger pieces of mafic magma are enclosed in such a halo. Thus, the filament presented in Figure 9D was probably still stretching when the sample was quenched, leaving a sharp contact. In contrast, the filament with progressive contacts is separated from the main layer by a sodic plagioclase-rich magma (Fig. 9E, profile F). Thus, diffusion operated across the filament in PP176 (Fig.SI 3E, profile F) before the run was ended, implying that the deformation of this filament was stopped, or at least slowed down, allowing chemical diffusion. The occurrence of the plagioclase halo on one side of the filament (Fig. 9E) may have damped deformation in that region of the sample. Our experiments illustrate that filaments expelled out of the mafic layer or enclave and suffering large strains produce schlierens, layering (Fig. 12C-4), chemically banded magma (Fig. 12C-5), which eventually ends producing a fully mixed hybrid magma upon repeated folding and stretching (Fig. 12C-6, -7; Perugini et al., 2003).

4.6. Quantification of the mixing process from textural/chemical observations

As highlighted above, once a given lower crystallinity threshold is reached, mingling and mixing textures develop as soon as strain affects the system. The range of plagioclase composition (Fig. 5a), the presence of plagioclases and pyroxenes out of equilibrium with no chemical gradient in the glass at their immediate contact (Fig. 11), all witness the rapidity of mixing processes under our experimental conditions. Results presented here are to some extent specific to the chemical gradient between the juxtaposed magmas and the conditions applied during experiments. Experiments produced under the same conditions (e.g. at 1170°C, and similar strain rate) all yielded similar mixing features (Fig. 8). No obvious relationships between either a particular texture or a chemical attribute could be established with time or with the strain of the experiment (Fig.SI 3): for

instance, isolated xenocrysts occur along with enclaves or melt filaments in the same experiment: hence it cannot be said that enclaves typify a lower amount of strain than isolated xenocrysts occurrence. This is perhaps in part related to the relatively low amount of finite strain reached in our experiments. However, for the time being, it appears difficult to relate any specific texture to a given strain amount or to a particular regime.

5. CONCLUSIONS

Torsion experiments conducted on dry hapltonalite and basalt under conditions relevant to natural situations shed light on the conditions required for magma mixing and the development of typical mingling and mixing features commonly observed in magmatic rocks. In accord with previous studies (e.g., [Philpotts et al., 1995](#); [Martin et al., 2006a](#)), the crystal content of a magma appears to be a critical parameter controlling its mixing capacities, due to its effect on the viscosity of magmas. With the crystal shape ratios characteristic of our starting mafic material, it appears that a crystal fraction exceeding ~50% is required to maintain a touching crystal framework which hinders the co-deformation of both end-members and any consequent mixing, the bulk of deformation being essentially concentrated in the less viscous magma. Below this threshold, which happens over a 10°C temperature interval, the mafic magma starts to disrupt producing simultaneous mingling and mixing textures (finger-like pattern, enclaves, stretched filament, intermediate melts and crystals in disequilibrium with their host). The mixing process also results in the crystallization of crystals showing normal (plagioclase) and reverse (olivine, pyroxene) zoning patterns. Generally, a particular texture is not linked to a specific deformation parameter such as strain rate or amount of deformation, except for the case of melt filaments that developed at the highest strain rates investigated. So, it appears difficult, if even possible, to quantify strain, strain rate or residence time from textural mixing or mingling features. The threshold established in this study is by no means universal: it will depend, as already stressed, on the average particle axial ratio of the suspension being strained, but also on the possible occurrence of bubbles ([Martin et al.,](#)

2006a), hence on the volatile content of the magmas prior to mixing. Therefore, additional studies such as the present one are required before a comprehensive model of magma mixing can be proposed.

FUNDING

This work was supported by the French Agence National de Recherche [ANR-08CEA080 to B. S].

ACKNOWLEDGEMENTS

This paper is a part of ML's PhD. The authors are grateful to T. Druitt for help on the field and J. Andújar for basalt sampling and discussion. We thank I. Di Carlo for help in EMP analyses, M. Drignon for the Santorini basalt characterization and E. Lemoing and P. Teulat for technical assistance. The paper greatly benefited from exhaustive reviews of Madeleine Humphreys and an anonymous reviewer.

REFERENCES CITED

- Albertz, M., Paterson, S.R., Okaya, D. (2005). Fast strain rates pluton emplacement: Magmatically folded leucocratic dikes in aureoles of the Mount Stuart Batholith, Washington, and the Tuolumne Intrusive Suite, California, *Geological Society of America Bulletin* **117**, 450-465.
- Anderson, A.T. (1976). Magma mixing: petrological process and volcanological tool, *Journal of Volcanology and Geothermal Research* **1**, 3-33, doi:10.1016/0377-0273(76)90016-0.
- Andújar, J., Scaillet, B., Druitt, T.H., Pichavant, M. (in preparation for *Journal of Petrology*). Differentiation conditions of a basaltic magma from Santorini and its bearing on basaltic-andesite to andesitic magma production.
- Appel, P.W.U., Polat, A., Frei, R. (2009). Dacitic ocelli in mafic lavas, 3.8-3.7 Ga Isua greenstone belt, West Greenland : geochemical evidence for partial melting of oceanic crust and magma mixing. *Chemical Geology* **258**, 105-124, doi:10.1016/j.chemgeo.2008.09.011.

- Armienti, P., Barberi, F., Bizouard, H., Clocchiatti, R., Innocenti, F., Metrich, N., Rosi, M., Sbrana, A. (1983). The phlegraean fields: Magma evolution within a shallow chamber. *Journal of Volcanology and Geothermal Research* **17** (1-4), 289-311, DOI: 10.1016/0377-0273(83)90073-2.
- Arzi, A.A. (1978). Critical phenomena in the rheology of partially melted rocks. *Tectonophysics* **44**, 173-184.
- Bacon, C. R. (1986). Magmatic Inclusions in Silicic and Intermediate Volcanic Rocks. *Journal of Geophysical Research* **91** (B6), 6091–6112, doi:10.1029/JB091iB06p06091.
- Barbarin, B. (2005). Mafic magmatic enclaves and mafic rocks associated with some granitoids of the central Sierra Nevada batholith, California: nature, origin, and relations with the hosts. *Lithos* **80**, 155-177.
- Barbey, P., Gasquet, D., Pin, C., Bourgeix, A.L. (2008). Igneous banding, schlieren and mafic enclaves in calc-alkaline granites: The Budduso pluton (Sardinia). *Lithos* **104**, 147-163.
- Barnhoorn, A., Bystricky, M., Kunze, K., Burlini, L., & Burg, J. P. (2005). Strain localisation in biminerale rocks: experimental deformation of synthetic calcite–anhydrite aggregates. *Earth and Planetary Science Letters*, *240*(3), 748-763.
- Bergantz, G.W. (2000). On the dynamics of magma mixing by reintrusion: implication for pluton assembly processes. *Journal of Structural Geology* **22**, 1297-1309.
- Blake, S. (1984). Magma mixing and hybridization processes at the alkalic, silicic, Torfajokull central volcano triggered by tholeiitic Veidivotn fissuring, south Iceland. *Journal of Volcanology and Geothermal Research* **22** (1-2), 1-31, DOI: 10.1016/0377-0273(84)90033-7.
- Blake, S., Ivey, G.N. (1986). Magma-mixing and the dynamics of withdrawal from stratified reservoirs. *Journal of Volcanology and Geothermal Research* **27** (1-2), 153-178, DOI: 10.1016/0377-0273(86)90084-3.
- Browne, B.L., Eichelberger, J.C., Patino, L.C., Vogel, T.A., Uto, K., Hoshizumi, H. (2006). Magma mingling as indicated by texture and Sr / Ba ratios of plagioclase phenocrysts from Unzen volcano, SW Japan. *Journal of Volcanology and Geothermal Research* **154** (1-2) 103-116, DOI: 10.1016/j.jvolgeores.2005.09.022.
- Carroll, M. R., & Wyllie, P. J. (1989). Granite melt convecting in an experimental micro-magma chamber at 1050 degrees C, 15 kbar. *European Journal of Mineralogy* **1**(2), 249-260.
- Caricchi, L., Giordano, D., Burlini, L., Ulmer, P., & Romano, C. (2008). Rheological properties of magma from the 1538 eruption of Monte Nuovo (Phlegrean Fields, Italy): An experimental study. *Chemical Geology* **256** (3), 158-171.
- Caricchi, L., C. Annen, A. Rust, Blundy, J. (2012). Insights into the mechanisms and timescales of pluton assembly from deformation patterns of mafic enclaves. *Journal of Geophysical Research*, doi:10.1029/2012JB009325.

- Castro, A., De La Rosa, J.D., Stephens, W.E. (1990). Magma mixing in the subvolcanic environment: petrology of the Gerena interaction zone near Seville, Spain. *Contributions to Mineralogy and Petrology* **106**, 9-26, Doi:10.1007/BF00306405.
- Civetta, L., Galati, R., Santacroce, R. (1991). Magma mixing and convective compositional layering within the Vesuvius magma chamber. *Bulletin of Volcanology* **53** (4), 287-300, DOI: 10.1007/BF00414525.
- Civetta, L., Orsi, G., Pappalardo, L., Fisher, R.V., Heiken, G., Ort, M. (1997). Geochemical zoning, mingling, eruptive dynamics and depositional processes--the Campanian ignimbrite, Campi Flegrei Caldera, Italy. *Journal of Volcanology and Geothermal Research* **75**, 183–219, doi:10.1016/S0377-0273(96)00027-3.
- Clynne, M.A. (1999). A Complex Magma Mixing Origin for Rocks Erupted in 1915, Lassen Peak, California. *Journal of Petrology* **40** (1), 105-132, doi: 10.1093/ptro/40.1.105.
- Coombs, M.C., Eichelberger, J.C., Rutherford, M.J. (2002). Experimental and textural constraints in mafic enclave formation in volcanic rocks. *Journal of Volcanology and Geothermal Research* **119**, 125-144, doi:10.1016/S0377-0273(02)00309-8.
- Costa, A., Caricchi, L., & Bagdassarov, N. (2009). A model for the rheology of particle-bearing suspensions and partially molten rocks. *Geochemistry, Geophysics, Geosystems*, *10*(3).
- Davi, M., De Rosa, R., Holtz, F. (2010). Mafic enclaves in the rhyolitic products of Lipari historical eruptions; relationships with the coeval Vulcano magmas (Aeolian Islands, Italy). *Bulletin of Volcanology* **72** (8), 991-1008, DOI: 10.1007/s00445-010-0376-5.
- De Campos, C.P., Dingwell, D.B., Perugini, D., Civetta, L., Fehr, T.K. (2008). Heterogeneities in magma chambers: Insights from the behavior of major and minor elements during mixing experiments with natural alkaline melts. *Chemical Geology* **256**, 131-145.
- De Campos, C.P., Perugini, D., Ertel-Ingrisch, W., Dingwell, D.B., Poli, G. (2011). Enhancement of magma mixing efficiency by chaotic dynamics :an experimental study. *Contributions to Mineralogy and Petrology* **161**, 863-881.
- De Rosa, R., Mazzuoli, R., Ventura, G. (1996). Relationships between deformation and mixing processes in lava flows: a case study from Salina (Aeolian Islands, Tyrrhenian Sea). *Bulletin of Volcanology* **58**, 286-297, DOI: 10.1007/s004450050140.
- De Rosa, R., Donato, P., Ventura, G. (2002). Fractal analysis of mingled/mixed magmas: an example from the Upper Pollara eruption (Salina Island, southern Tyrrhenian Sea, Italy). *Lithos* **65**, 299-311.
- Di Carlo, I., Pichavant, M., Rotolo, S.G., Scaillet, B. (2006). Experimental crystallization of a high-K arc basalt: The golden pumice, Stromboli volcano (Italy). *Journal of Petrology* **47**, 1317-1343.

- Dokukina, K.A., Konilov, A.N., Kaulina, T.V., Vladimirov, V.G. (2010). Interaction between mafic and felsic magmas in subvolcanic environment (Tastau igneous complex, eastern Kazakhstan). *Russian Geology and Geophysics* **51**(6), 625-643, DOI: 10.1016/j.rgg.2010.05.004.
- Druitt, T.H., Edwards, L., Mellors, R.M., Pyle, D.M., Sparks, R.S.J., Lanphere, M., Davies, M., Barriero, B. (1999). Santorini Volcano. *Journal of Geological Society of London, Memoir* 19, pp165.
- Druitt, T.H., Costa, F., Deloule, E., Dungan, M., Scaillet, B. (2012). Decadal to monthly timescales of magma transfer and reservoir growth at a caldera volcano., *Nature* **482**, 77-80.
- Eichelberger, J.C. (1980). Vesiculation of mafic magma during replenishment of silicic magma reservoirs. *Nature* **288**, 446-450.
- Eichelberger, J.C., Izbekov, P. (2000). Eruption of andesite triggered by dike injection: Contrasting cases at Karymsky Volcano, Kamchatka and Mount Katmai, Alaska. *Royal society of London Philosophical transactions, ser. A, v.* **358**, 1465-1485.
- Eichelberger, J.C. (2010). Messy magma mixtures. *Nature Geoscience* **3**, 593-594, doi:10.1038/ngeo951.
- Erdmann, S., Scaillet, B., Kellet, A. (2012). Textures of peritectic crystals as guides to reactive minerals in magmatic systems: new insights from melting experiments. *Journal of Petrology* **53**, 2231-2258.
- Ghiorso, M. S., Sack, R. O. (1995). Chemical Mass Transfer in Magmatic Processes. IV. A Revised and Internally Consistent Thermodynamic Model for the Interpolation and Extrapolation of Liquid-Solid Equilibria in Magmatic Systems at Elevated Temperatures and Pressures. *Contributions to Mineralogy and Petrology* **119**, 197-212
- Giordano, D., Russell, J.K., and Dingwell, D.B. (2008). Viscosity of magmatic liquids: A model. *Earth and Planetary Science Letters* **271** (1-4), 123–134, doi: 10.1016/j.epsl.2008.03.038.
- Hodge, K.F., and Jellinek, A.M. (2012). Linking enclave formation to magma rheology. *Journal of geophysical Research* 117, B10208, doi: 10.1029/2012JB00393.
- Holloway, J.R., Dixon, J.E., Pawley, A.R. (1992). An internally heated, rapid quench, high pressure vessel. *American Mineralogist* **77**, 643-646.
- Holtz, F., Sato, H., Lewis, J., Behrens, H., Nakada, S. (2005). Experimental petrology of the 1991–1995 Unzen dacite, Japan. part I: phase relations, phase composition and preeruptive conditions. *Journal of Petrology* **46**, 319-337, doi: 10.1093/petrology/egh077.
- Huppert, H.E., Stephen, R., Sparks, R.S.J., Turner, J.S. (1984). Some effects of viscosity on the dynamics of replenished magma chambers. *Journal of Geophysical Letter* **89** (B8), 6857-6877, doi:10.1029/JB089iB08p06857.
- Jellinek, M., Kerr, R.C. (1999). Mixing and compositional stratification produced by natural convection, 2. Applications to the differentiation of basaltic and silicic magma chambers and komatiites lava flows. *Journal of Geophysical Research* **104**, 7203-7218.

- Kent, A.J.R., Darr, C., Koleszar, A.M., Salisburry, M.J., Cooper, K.M. (2010). Preferential eruption of andesitic magmas through recharge filtering. *Nature Geoscience* **3**, 631-636.
- Kouchi, A., Sunagawa, I., (1982). Experimental study of mixing of basaltic and dacitic magmas. *Science Reports of the Tohoku University*, ser. 3, vol. **15**, 163-175.
- Kouchi, A., Sunagawa, I. (1985). A model for mixing basaltic and dacitic magmas as deduced from experimental data. *Contributions to Mineralogy and Petrology* **89**, 17–23, DOI: 10.1007/BF01177586.
- Koyaguchi, T., Blake, S. (1989). The dynamics of magma mixing in a rising magma batch. *Bulletin of Volcanology* **52**, 127–137, DOI: 10.1007/BF00301552.
- Kuscu, G.G., Floyd, P.A. (2001). Mineral compositional and textural evidence for magma mingling in the saraykent volcanics. *Lithos* **56**, 207-230, doi:10.1016/S0024-4937(00)00051-7.
- La Felice, S., Landi, P. (2011). The 2009 paroxysmal explosions at Strombolie (Italy): magma mixing and eruption dynamics. *Bulletin of Volcanology* **73**, 1147-1154.
- Lange, R.A., Carmichael, I.S.E. (1990). Thermodynamics properties of silicate liquids with emphasis on density, thermal expansion and compressibility, in *Modern Methods in igneous petrology: understanding magmatic processes*, Rev. Mineral. 24, edited by J. Nicholls and J.K. Russell, 25-64, Mineral Society of America, Washington D.C.
- Laumonier, M., Arbaret, L., Burgisser, A., & Champallier, R. (2011). Porosity redistribution enhanced by strain localization in crystal-rich magmas. *Geology*, *39*(8), 715-718.
- Laumonier, M., Scaillet, B., Arbaret, L., Andújar, J., Champallier, R. (submitted to *Chemical Geology*). Experimental mixing of hydrous crystal-bearing magmas.
- Laumonier, M., Scaillet, B., Arbaret, L., Champallier, R. (in preparation). On the condition of mafic-felsic magma mixing.
- Launeau, P. (2004). Mise en évidence des écoulements magmatiques par analyse d'image 2-D des distributions 3-D d'Orientations Préférentielles de Forme. *Bulletin de la Société Géologique de France* **175**, 331-350. (« Magmatic flows brought to light by 2-D image analysis of the distribution of 3-D Shape Preferred Orientation »).
- Mandeville, C.W., Carey, S., Sigurdsson, H. (1996). Magma mixing, fractional crystallization and volatile degassing during the 1883 eruption of Krakatau volcano, Indonesia. *Journal of Volcanology and Geothermal Research* **74** (3-4), 243-274, DOI: 10.1016/S0377-0273(96)00060-1.
- Martel, C., Ali, A.R., Poussineau, S., Gourgaud, A., Pichavant, M. (2006). Basalt-inherited microlites in silici magmas : Evidence from Mount Pelée (Martinique, French West Indies). *Geology* **34**, 905-908.
- Martel, C., Poussineau, S. (2007). Diversity of eruptive styles inferred from the microlites of Mt Pelée andesite (Martinique, Lesser Antilles). *Journal of Volcanology and Geothermal Research* **166**, 233-254.

- Martin, V.M., Holness, M.B., Pyle, D.M. (2006a). The role of crystal frameworks in the preservation of enclaves during magma mixing. *Earth and Planetary Science Letters* **248**, 787-799.
- Martin, V.M., Holness, M.B., Pyle, D.M. (2006b). Textural analysis of magmatic enclaves from the Kameni Islands, Santorini, Greece. *Journal of Volcanology and Geothermal Research* **154** (1-2), 89-102, DOI:10.1016/j.jvolgeores.2005.09.021.
- McKenzie, D. (1984). The generation and compaction of partially molten rock. *Journal of Petrology* **25**, 713-764.
- Miller, T.P., Chertkoff, D.G., Eichelberger, J.C., Coombs, M.L. (1999). Mount Dutton Volcano, Alaska: Aleutian Arc analog to Unzen volcano, Japan. *Journal of Volcanology and Geothermal Research* **89**, 275-302.
- Morgavi, D., Perugini, D., De Campos, C. P., Ertl-Ingrisch, W., Lavallée, Y., Morgan, L., & Dingwell, D. B. (2012). Interactions between rhyolitic and basaltic melts unraveled by chaotic mixing experiments. *Chemical Geology*.
- Nakamura, M. (1995). Continuous mixing of crystal mush and replenished magma in the ongoing Unzen eruption. *Geology* **23**, 807–810, doi: 10.1130/0091-7613.
- Nicholls, I. A. (1971). Petrology of Santorini Volcano, Cyclades, Greece. *Journal of Petrology* **12** (1), 67-111
- Pal, T., Mitra, S.K., Sengupta, S., Katari, A., Bandopadhyay, P.C., Bhattacharya, A.K. (2007). Dacite-andesite of Narcondam volcano in the Andaman sea – An imprint of magma mixing in the inner arc of the Andaman-Java subduction system. *Journal of Volcanology and Geothermal Research* **168**, 93-113, doi:10.1016/j.jvolgeores.2007.08.005.
- Pallister, J.S., Hoblitt, R.P., Meeker, G.P., Knight, R.J., and Siems, D.F. (1996). Magma mixing at Mount Pinatubo: Petrographic and chemical evidence from 1991 deposits, in Newhall, C., and Punongbayan, R., eds., *Fire and Mud: Eruptions and Lahars of Mount Pinatubo: Quezon City, Philippine Institute of Volcanology and Seismology, and Seattle, University of Washington Press*, 687-732.
- Paterson, M., Olgaard, D. (2000). Rock deformation tests to large shear stress in torsion. *Journal of Structural Geology* **22**, 1341-1358, doi:10.1016/S0191-8141(00)00042-0.
- Paterson, S.R., Pignotta, G.S., Vernon, R.H. (2004). The significance of microgranitoid enclave shapes and orientations. *Journal of Structural Geology* **26**, 1465-1481.
- Perugini, D., Busa, T., Poli, G., Nazzareni, S. (2003). The role of chaotic dynamics and flow fields in the development of disequilibrium textures in volcanic rocks. *Journal of Petrology* **44**, 733-756.
- Perugini, D., Ventura, G., Petrelli, M., Poli, G. (2004). Kinematic significance of morphological structures generated by mixing of magmas: a case study from Salina Island (Southern Italy). *Earth and Planetary Science Letters* **222**, 1051-1066, doi:10.1016/j.epsl.2004.03.038.
- Perugini, D., Poli, G. (2005). Visous fingering during replenishment of felsic magma chambers by continuous inputs of mafic magmas: Field evidence and fluid-mechanics experiments. *Geology* **33**, 5-8.

- Perugini, D., Poli, G. (2012). The mixing of magmas in plutonic and volcanic environment: Analogies and differences. *Lithos*, DOI:10.1016/j.lithos.2012.02.002.
- Petford, N. (1996). Dykes or diapers? *Royal Society of Edinburgh Transactions, Earth Sciences* **87**, 105-114.
- Pin, C., Binon, M., Belin, J.M., Barbarin, B., Clemens, J.D. (1990). Origin of microgranular enclaves in granitoids: equivocal Sr-Nd evidence from Hercynian rocks in the Massif Central (France). *Journal of Geophysical Research* **95** (B11), 17 821:17828.
- Philpotts, A.R., Shi, J., Brustman, C. (1998). Role of plagioclase crystal chains in the differentiation of partly crystallized basaltic magma. *Nature* **395**, 343-346.
- Picard, D. (2009). HP-HT deformation of silicic magmas: experimental constraints on the structural evolution and the rheological threshold at middle and high crystallinities, PhD thesis, University of Orleans (FR), pp.334.
- Picard, D., Arbaret, L., Picahvant, M., Champallier, R., Launeau, P. (2011). Rheology and microstructures of experimentally plagioclase suspensions. *Geology* **39**, 747-750.
- Pons, J., Barbey, P., Nachit, H., Burg, J.P. (2006). Development of Igneous layering during growth of pluton: the Tarçouate Laccolith (Morocco). *Tectonophysics* **413**, 271-286.
- Roscoe, R. (1952). The viscosity of suspensions of rigid spheres. *British Journal of Applied Physics* **3**, p267-269.
- Rosenberg, C.L., Handy, M.R. (2005). Experimental deformation of partially melted granite revisited: implications for the continental crust. *Journal of Metamorphic Geology* **23**, 19-28.
- Ruprecht, P., Bachmann, O. (2010). Pre-eruptive reheating during magma mixing at Quizapu volcano and the implications for the explosiveness of silicic arc volcano. *Geology* **38** (10), 919-922, doi:10.1130/G31110.1.
- Sakuyama, M. (1979). Evidence of magma mixing: petrological study of Shirouma-Oike calc-alkaline andesite volcano, Japan. *Journal of volcanology and Geothermal research* **5**, 179-208, doi:10.1016/0377-0273(79)90040-4.
- Sakuyama, M. (1984). Magma mixing and magma plumbing system in island arc. *Bulletin of Volcanology* **47** (4), 685-703, DOI: 10.1007/BF01952339.
- Sato, E., Sato, H. (2009). Study of effect of magma pocket on mixing of two magmas with different viscosities and densities by analogue experiments. *Journal of Volcanology and Geothermal Research* **181**, 115-123, doi:10.1016/j.jvolgeores.2009.01.005.
- Scaillet, B., Whittington, A., Martel, C., Picahvant, M., Holtz, F. (2000). Phase equilibrium constraints on the viscosity of silicic magmas with implications for mafic-silicic mixing processes. *Transactions of the Royal Society of Edinburgh: earth Sciences* **91**, 61-72.
- Smith, J.V. (2000). Structures on interfaces of mingled magmas, Stewart Island, New Zealand. *Journal of Structural Geology* **22**, 123-133, doi:10.1016/S0191-8141(99)00139-X.

- Sparks, S.R.J., Sigurdsson, H., and Wilson, L. (1977). Magma mixing: A mechanism for triggering acid explosive eruptions. *Nature* **267** (5609) 315-318, doi: 10.1038/267315a0.
- Sparks, R.S.J., Marshall, L.A. (1986). Thermal and mechanical constraints on mixing between mafic and silicic magmas. *Journal of Volcanology and Geothermal Research* **29**, 99–124, doi:10.1016/0377-0273(86)90041-7.
- Turnbull, R., Weaver, S., Tulloch, A., Cole, J., Handler, M., Ireland, T. (2010). Field and Geochemical Constraints on Mafic-Felsic Interactions, and Processes in High-level Arc Magma Chambers: an Example from the Halfmoon Pluton, New Zealand. *Journal of Petrology* **51**, 1477-1505.
- Turner, S., Foden, J. (1996). Magma mingling in late-Delamerian A-type granites at Mannum, South Australia. *Mineralogy and Petrology* **56**, 147-169.
- Van der Laan, S.R., Wyllie, P.J. (1993). Experimental interaction of granitic and basaltic magmas and implications for mafic enclaves. *Journal of Petrology* **34**, 491-517.
- Van der Molen, I., Paterson, M.S. (1978). Experimental deformation fo partially granite. *Contributions to Mineralogy and Petrology* **70**, 299-318.
- Venezky, D.Y., Rutherford, M.J. (1997). Preeruption conditions and timing of dacite-andesite magma mixing in the 2.2 ka eruption at Mount Rainier. *Journal of Geophysical Research* **102** (B9), 20,069-20,086, doi:10.1029/97JB01590
- Vigneresse, J.L., Barbey, P., Cuney, M. (1996). Rheological transition during partial melting and crystallization with application to felsic magma segregation and transfer. *Journal of Petrology* **37**, 1579-1600.
- Watson, E. B. (1982). Basalt contamination by continental crust: some experiments and models. *Contributions to Mineralogy and Petrology*, *80*(1), 73-87.
- Wiebe, R.A. (1996). Mafic-silicic layered intrusions: The role of basaltic injections on magmatic processes and the evolution of silicic chambers. *Royal Society of Edinburgh Transactions, Earth Sciences* **87**, 233-242.
- Williams, Q., Tobisch, O.T. (1992). Microgranitic enclave shapes and magmatic strain histories: Constraints from drop deformation theory. *Journal of Geophysical Research* **99**, B12, 24359-24368.
- Woods, A.W., Cowan, A. (2009). Magma mixing triggered during volcanic eruptions. *Earth and Planetary Science Letters* **288** (1-2) 132-137, DOI: 10.1016/j.epsl.2009.09.015.
- Zhang, Y., Walker, D., Leshner, C.E. (1989). Diffusive crystal dissolution. *Contribution to Mineralogy and Petrology* **102**, 492-513

FIGURES & FIGURE CAPTIONS

Figure 1 : Simple shear deformation occurring during reservoir replenishment and reproduced in torsion experiments. (A) Simple shear occurs between the rising dyke and the felsic host , at relatively high shear rate (10^{-5} to 10^{-2} s $^{-1}$; Albertz et al., 2005) compared to other magmatic environments (see the text for details). (B) Stack of sample geometry used for static and torsion experiments. The numbering of the disks extends from 1 (top) to 4 (bottom) and the colours grey and black refers to the felsic and the mafic end-members, respectively. The black arrows indicate the sense of shearing in the case of torsion experiments.

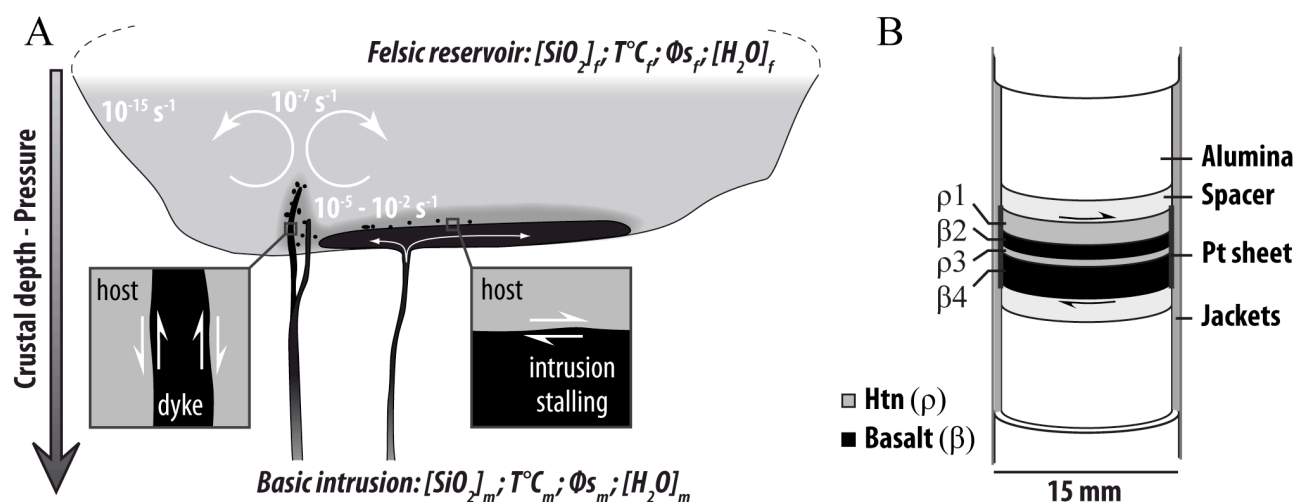


Figure 2: SEM pictures of the mafic starting material before experiments (A), after partial melting at 1170°C (B) and 1200°C (C). Pl=plagioclase, Px= Pyroxene; Ol=olivine; Ox=oxide; m=melt. Circles and stars refer to chemical analyses, described in later figures. The starting basalt SPO is shown by the yellow segments in (A). The segments define a fabric oriented in the rose diagram with the reference zero as the vertical. Numbers indicate the fabric intensity (regular font) and the number of segments (italic font).

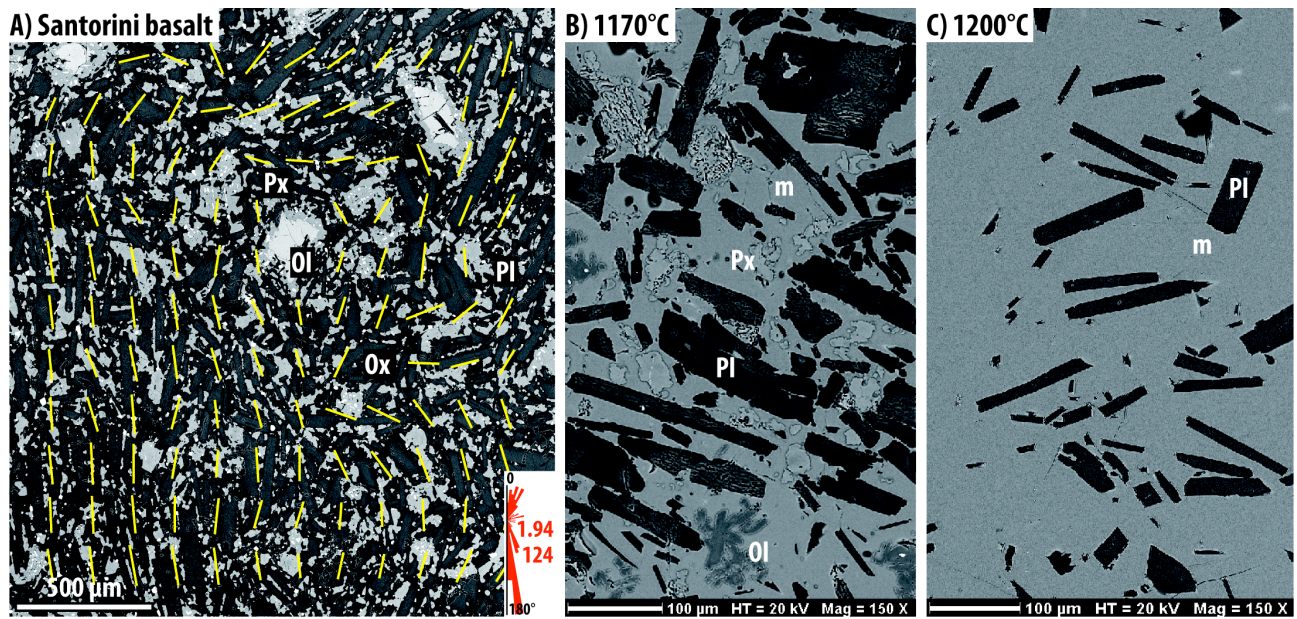


Figure 3: (A) Temperature vs crystal fraction of the basalt after 5-hour tests and comparison with the theoretical crystal fraction given by MELTS software (Ghiorso and Sack, 1995). (B) Melt and bulk viscosity calculated for each material taking into account the crystal fraction determined for temperatures ranging between 1000 and 1200°C. Melt and bulk viscosities of the felsic component are broadly the same, as long as the crystal fraction remains low (<10%) during the experiment. Note that the bulk viscosities of the end-members cross at a temperature close to 1170°C (black arrow).

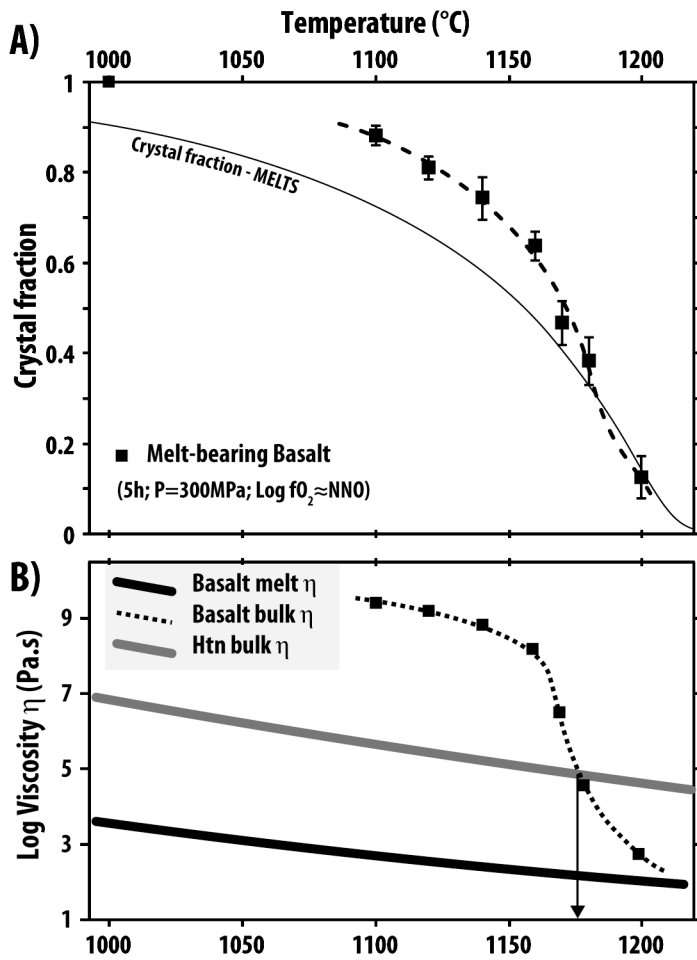
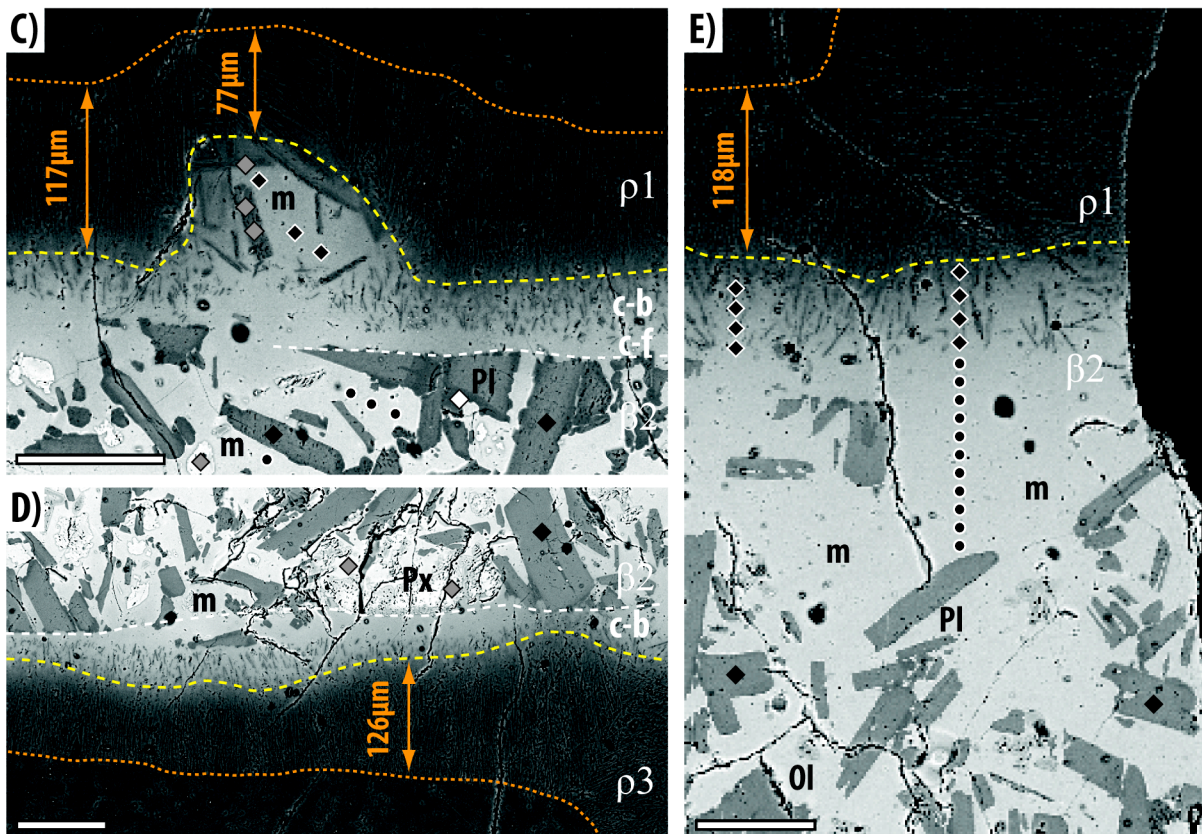
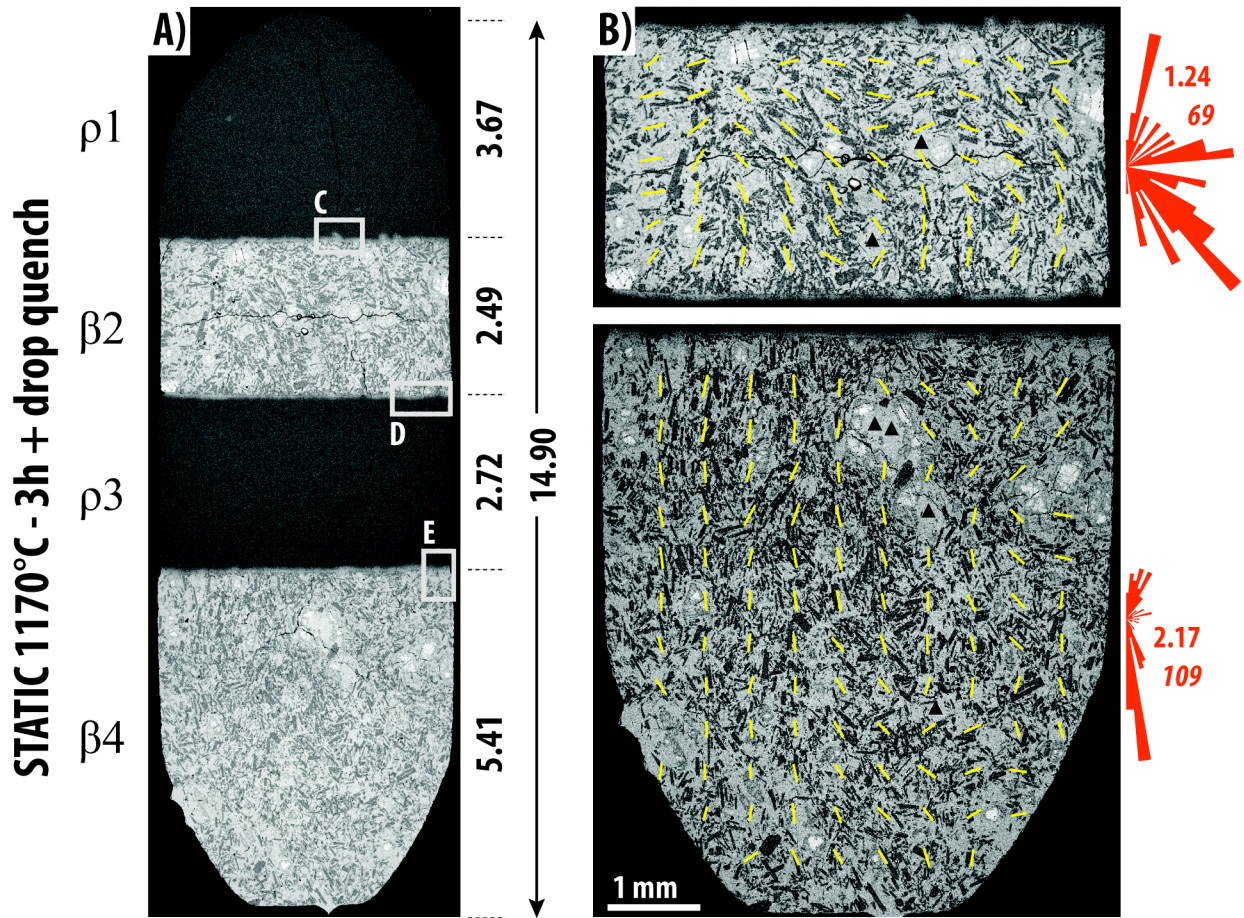


Figure 4 : Static runs conducted at 1170°C and 300 MPa for 3 (A to E) and 50 hours (F to I). (A) Disposition of the stack (image width is ~5 mm). (B) SPO (yellow segments) and fabric of the plagioclase crystals in each mafic layer (symbols as in legend of Fig. 1). (C, D and E) Detailed view of the interface between layers showing a plume, and local melt enrichment, and the thickness of the sodic plagioclase halo developing in the felsic layers. (F [xy] section showing the whole preserved structure and the thickness of the disks. (G) SPO (yellow segments) of the plagioclase crystals in each mafic layer. (H) Close up on the upper contact showing two different layers lying above the mafic disk: crystal-bearing (c-b) and crystal-free (c-f) layers are sandwiched between the two upper disks (β_1 and β_2) delimited by white dashed lines. Symbols are analytical spots as in the legend of the figure 6. (I) Close up on the lower contact with one layer sandwiched between the end-members. Letters between quotation marks are chemical profiles (see Fig. 6). The red dotted

line separates zones defined by the presence or not of quench crystals (q.c). (A and F) dimension in millimetres; (C, D, E, H and I) white bar represents 100 μm .



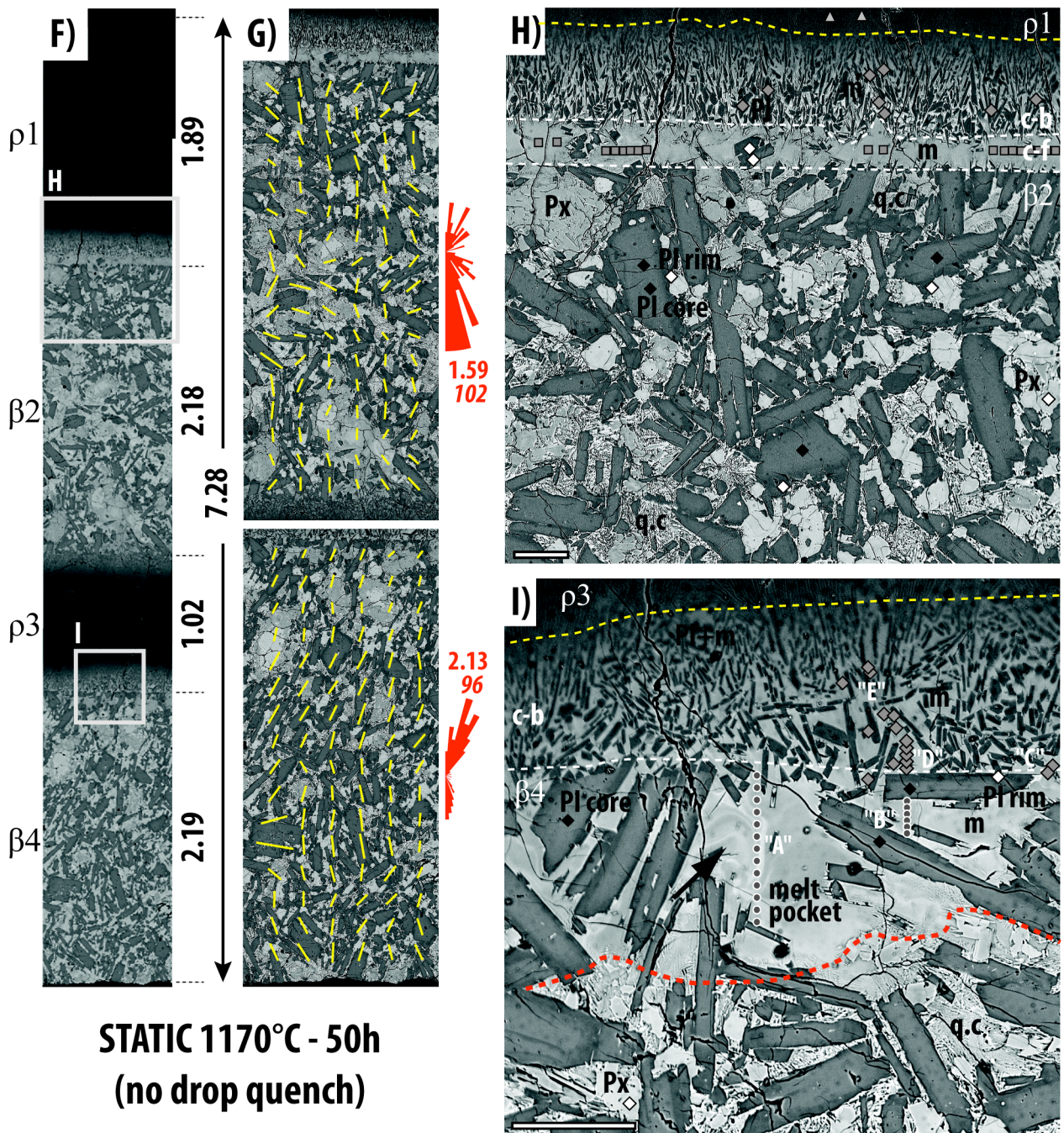


Figure 5: Analyses of plagioclase (A), pyroxenes (B & C), olivine (D) and melt (E & F) in Santorini basalt, static and torsion run products. “Isol.” stands for isolated, β refers to the mafic experimental products.

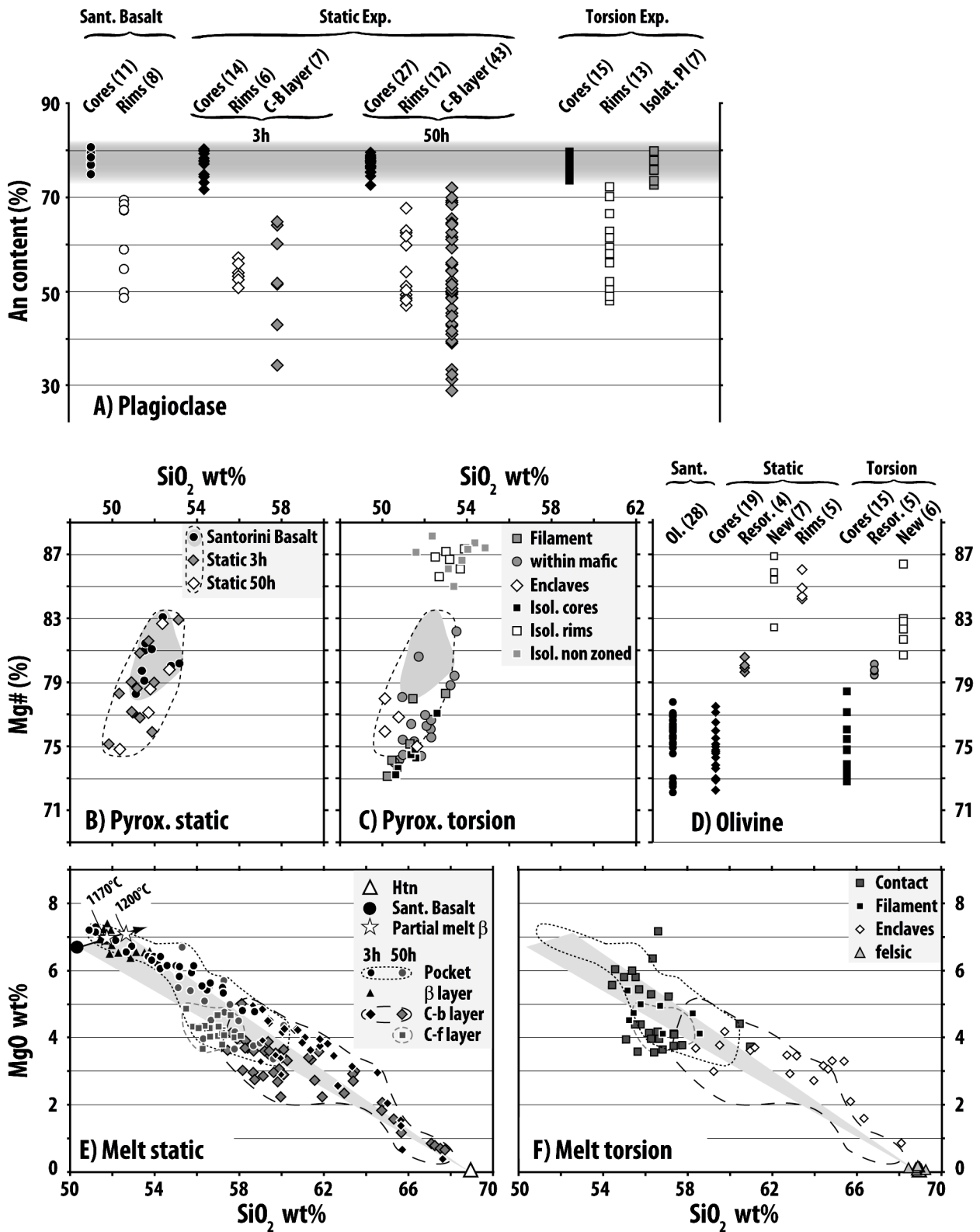


Figure 6: Chemical profiles of Si, Fe, Mg and Ca oxide concentrations from the initial contact between disks (grey line). The profiles are localized on Fig. 4I.

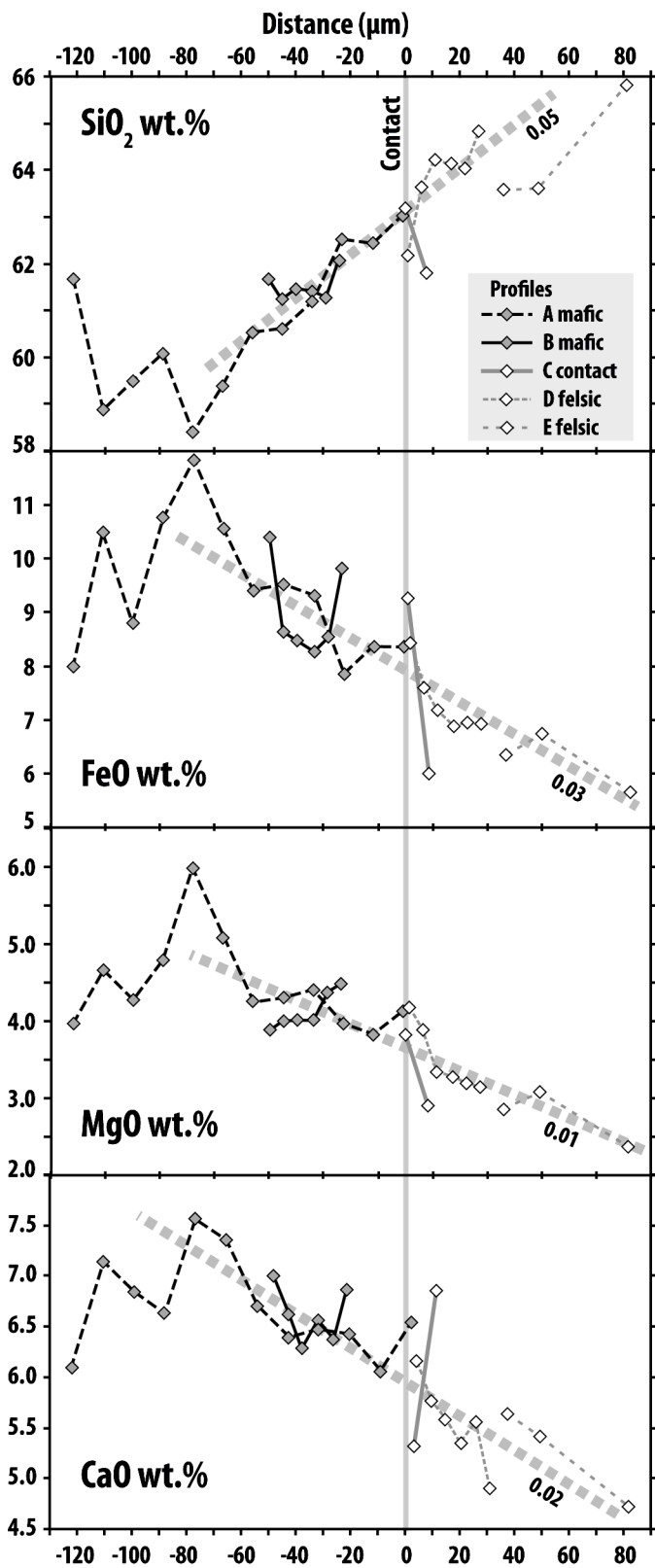
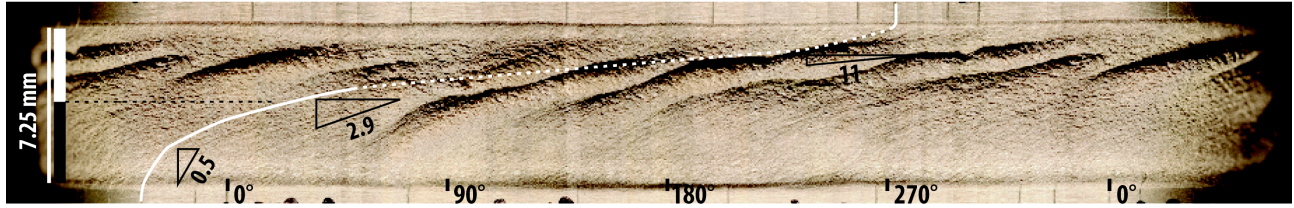


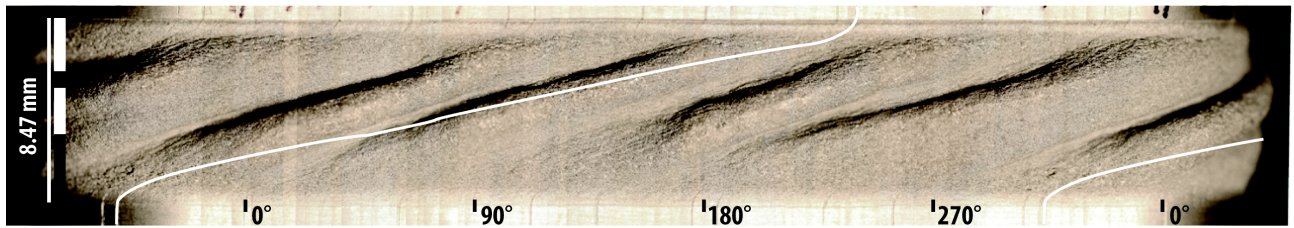
Figure 7: Reconstructed panorama displaying the external appearance of twisted samples still embedded in their iron jacket. The black and white rectangles represent the mafic and felsic initial distribution. The number in mm is the sample length, measured after experiments. Strain markers have been highlighted by a white line (dashed when not visible) and reveal the strain distribution

across the sample. For the PP156 experiment conducted at 1160°C, the strain is heterogeneously distributed and was locally calculated (triangles). Other experiments show a homogeneous strain distribution.

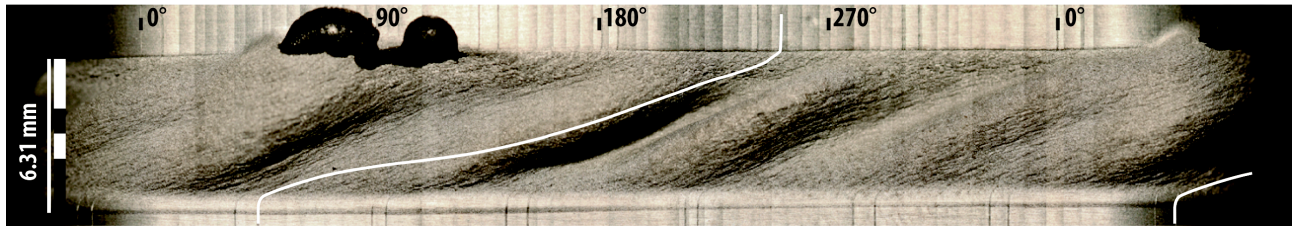
A) PP156 - 1160°C, $\gamma_{\text{bulk}} = 4.9$



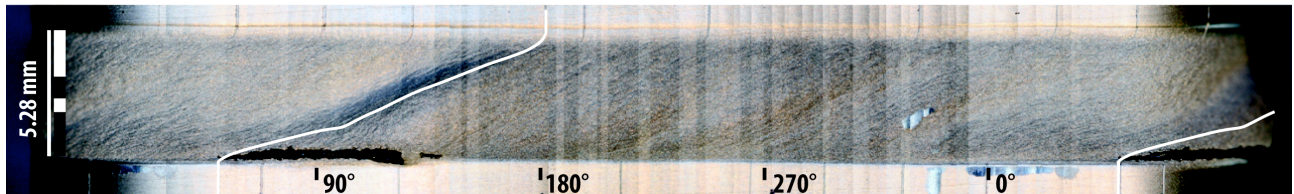
B) PP157 - 1170°C, $\gamma_{\text{bulk}} = 3.6$



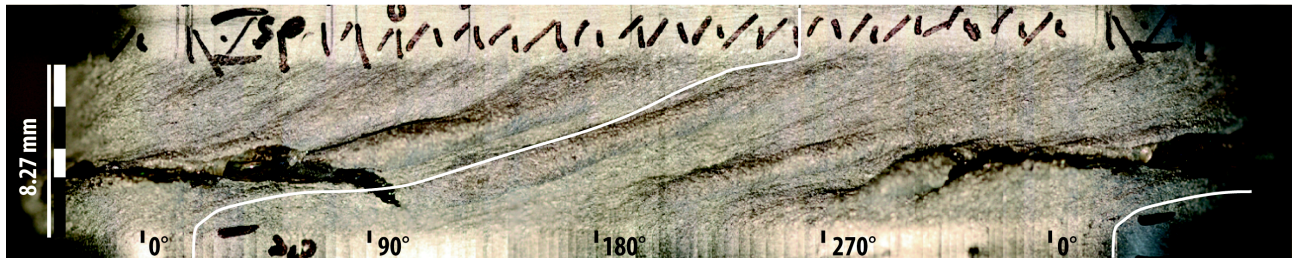
C) PP160 - 1170°C, $\gamma_{\text{bulk}} = 3.1$



D) PP161 - 1170°C, $\gamma_{\text{bulk}} = 3.1$



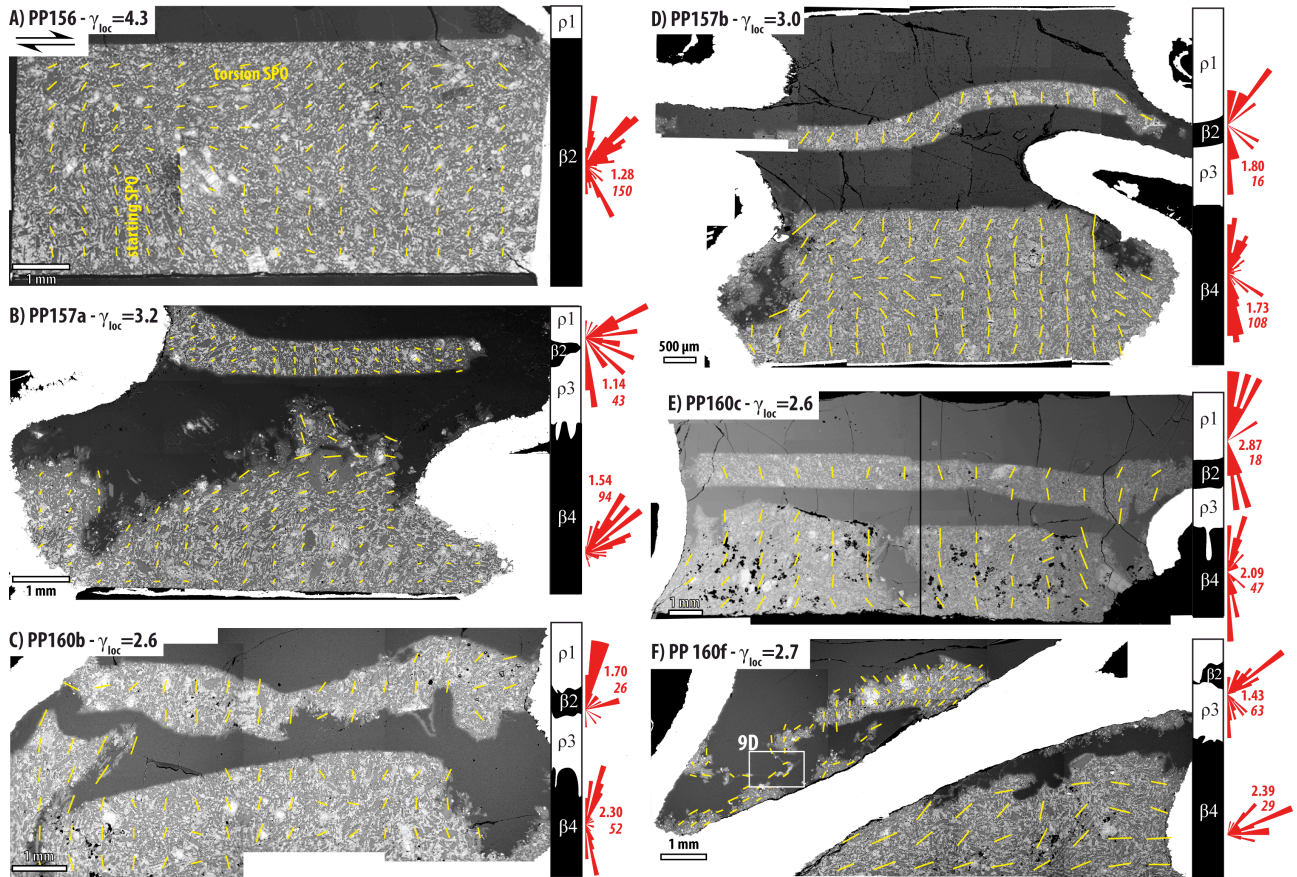
E) PP164 - 1170°C, $\gamma_{\text{bulk}} = 3.9$



F) PP176 - 1200°C, $\gamma_{\text{bulk}} = 3.8$



Figure 8: [xz] sections imaged by SEM showing the macroscopic shape of the layers (schematized on the right of each picture), the SPO (yellow segments) and the fabric distribution (rose diagram). The sense of shear is shown in (A). (I) The black and white dotted line shows the wavy contact between $\rho3$ and $\beta4$.



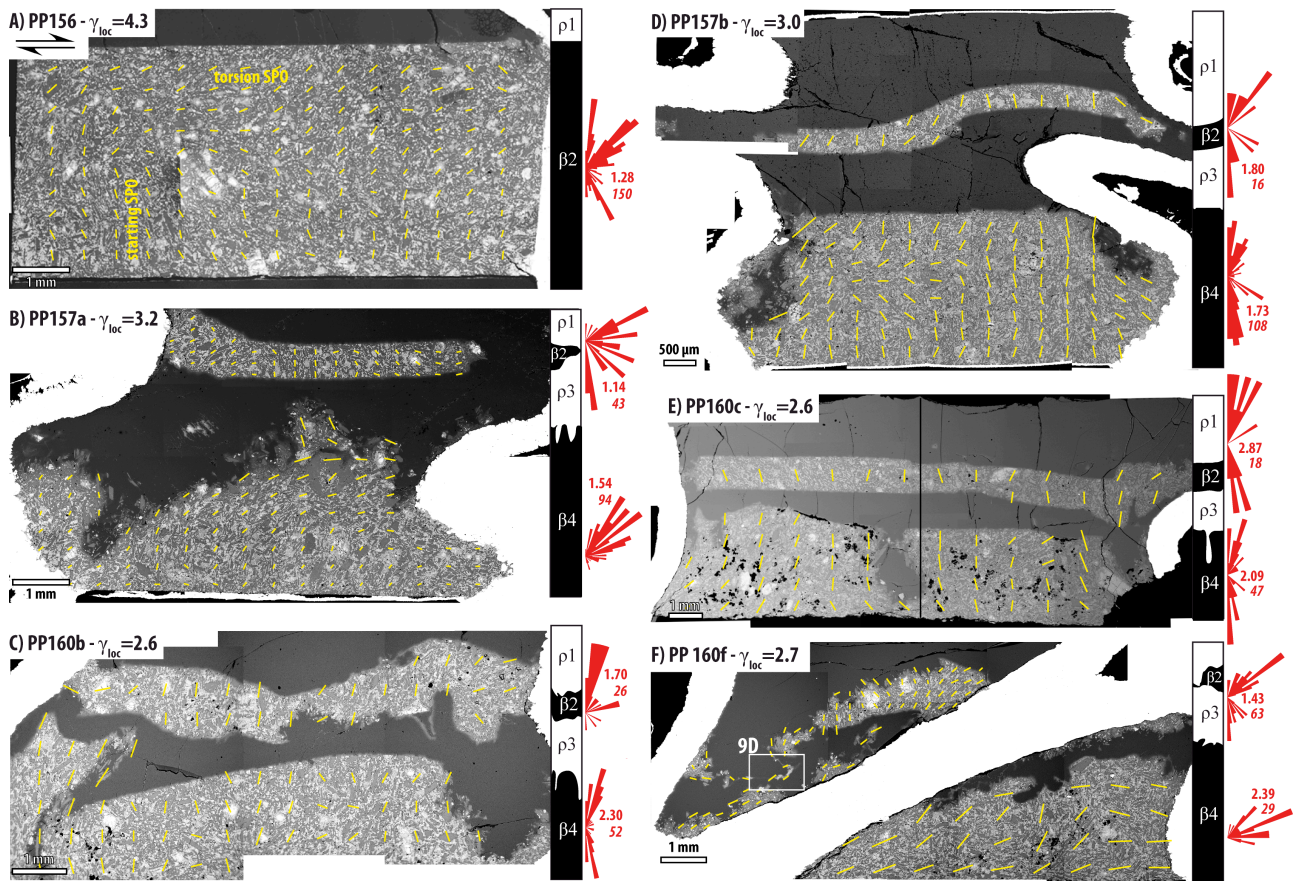


Figure 9: Detailed micro textures from [xz] sections of torsion experiments: mafic enclaves still connected to the main layer (A) and completely detached (B); felsic enclave (C); stretched filaments (D & E) and dispersed mafic crystals in the felsic component (F). In PP160, the stretched inclusion extends over 4.5 mm and carries some plagioclases whereas the stretched layer produced in PP176 is free of phenocrysts but has a progressive contact (white arrow). Letters in quotation marks stand for the chemical profiles in figures 13 and 14. Px n-z is non zoned pyroxene.

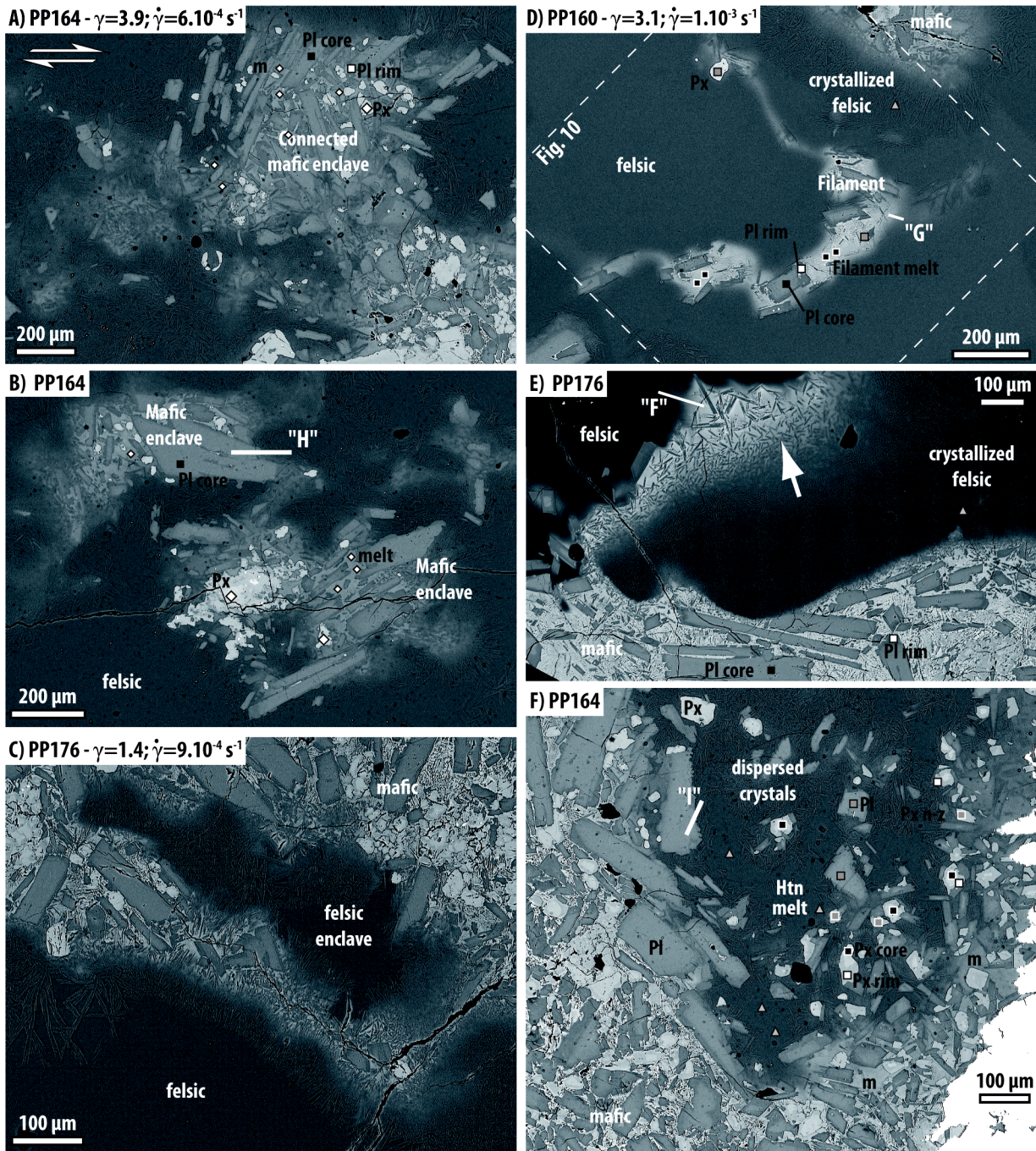
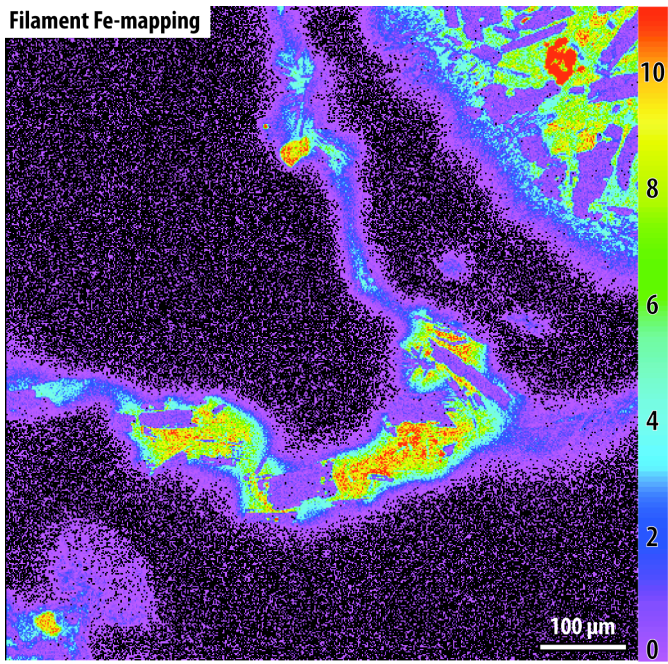
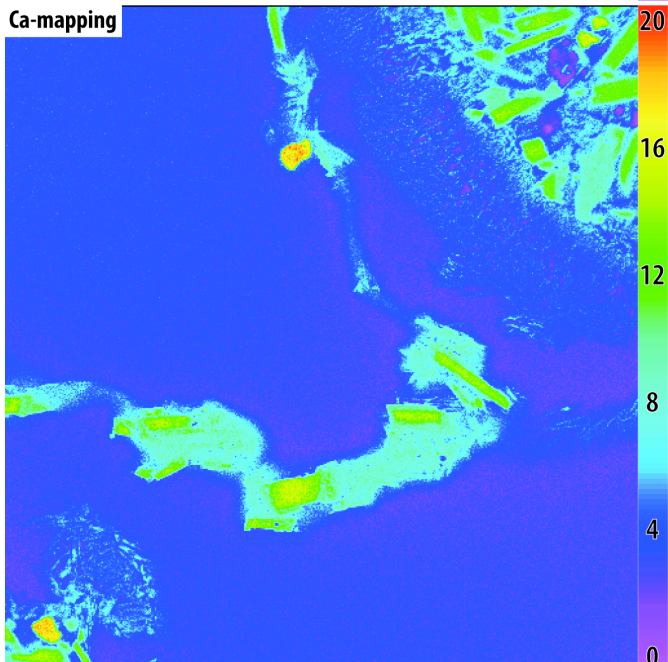


Figure 10: Iron, calcium & magnesium mapping of the melt filament produced PP160 (localisation in Fig. 9).

Filament Fe-mapping



Ca-mapping



Mg-mapping

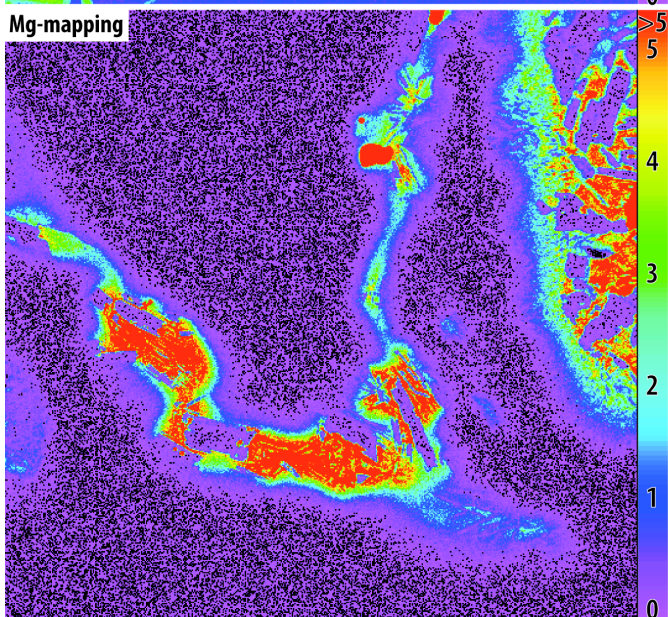


Figure 11: A) Chemical melt profiles for Si, Fe, Mg and Ca oxides at the borders of filaments (Fig.SI 3d, e). Numbers on the curves indicate the gradient of concentration in wt.%/μm. The zero is an arbitrary limit where the melt can be considered as of haplotonalitic composition. B) Chemical profiles at the interface plagioclase-melt (0 μm) for Si, Al, Ca and Na oxides for plagioclases located in an enclave (“H”) and in a felsic embayment (“I”).

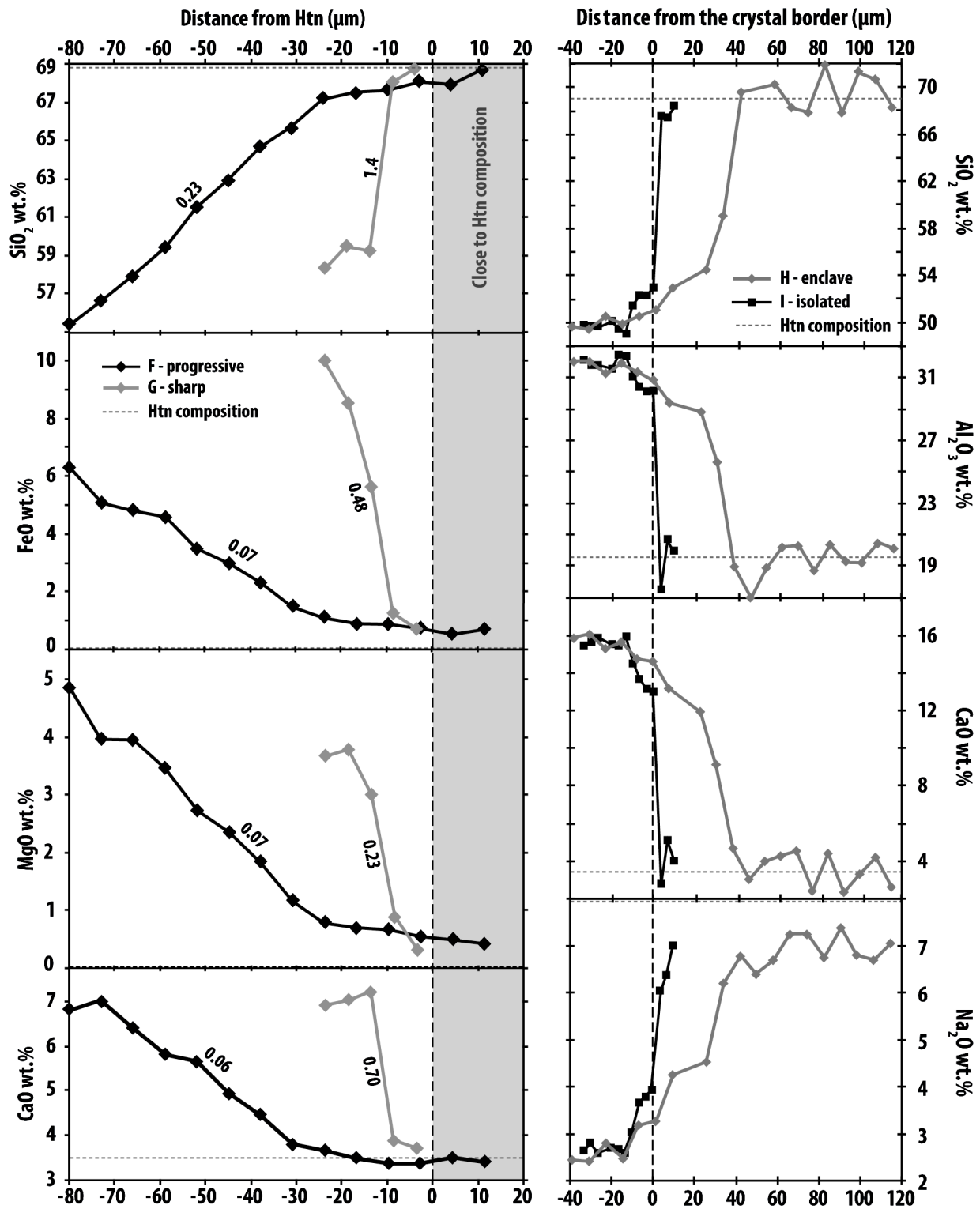


Figure 12: Sketch of the absence and presence of mingling and mixing features after torsion experiments. (A) Absence of any mixing or mingling texture when a component has an unbreakable crystal network. (B) Development of mingling textures (enclaves, isolated crystals) due to a

breakable crystal network and (C) mixing and mingling textures (filament, banded magmas, chaotic mixing, and hybrid) in magma without crystal network (crystal-poor). The different textures (number) are discussed in the text.

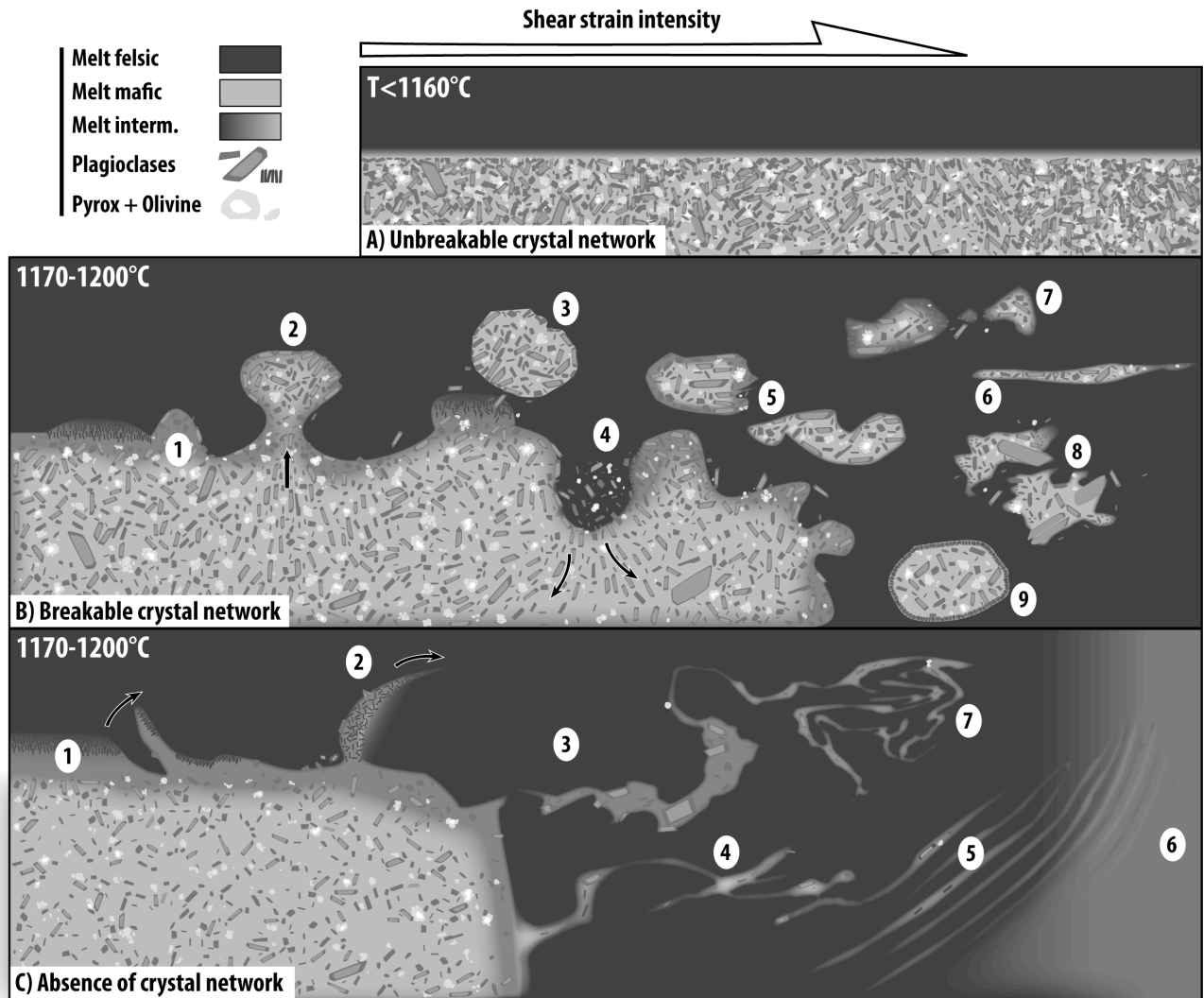


Figure SI 1: Cumulative fraction of the size distribution of the plagioclase long axes. Except for the starting material (Santorini basalt), the data concern experiments conducted at the same temperature (1170°C). Numbers in the legend are the number of plagioclases counted.

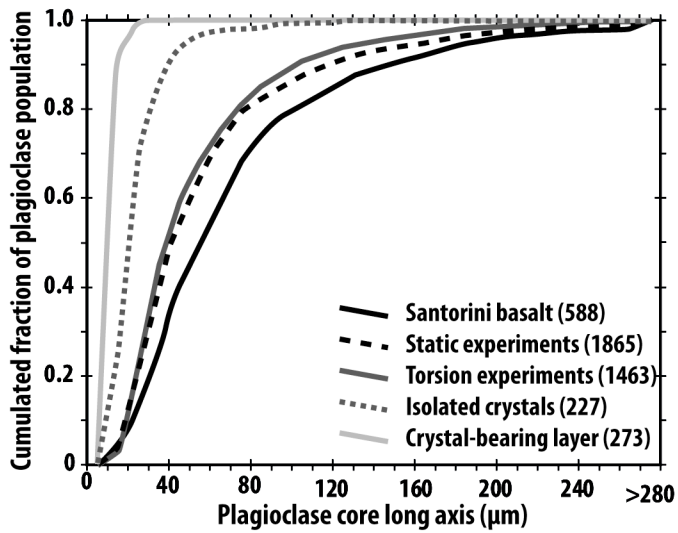


Figure SI 2: SEM images showing the different phases in the mafic layers in the 3-h static experiment. Core, rim, resorption and new olivines are in red (see also Fig. 5D) and other phases are in yellow (Pl: Plagioclase, Px: pyroxene, gl: glass).

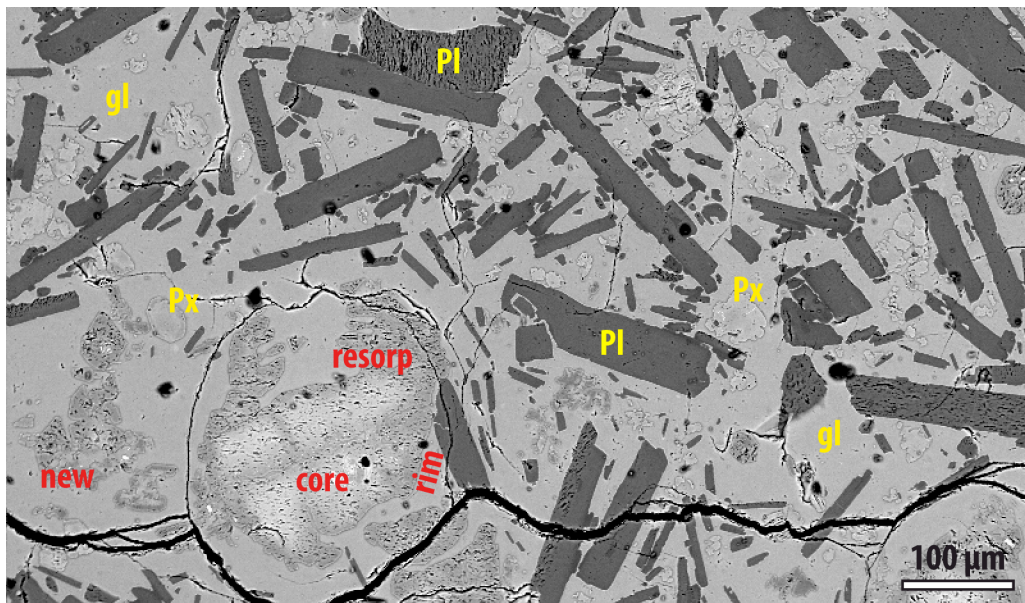


Figure SI 3: Local strain and strain rate vs. SPO intensity normalized to the Santorini basalt one of the mafic materials from starting basalt (SPO intensity = 1), static and torsion experiments. Strain and strain rate are null in the starting material and static experiments. Standard deviation of SPO intensity is lower than 2%.

